STABILITY OF NEUTRAL BEAM DRIVEN TAE MODES IN DIII-D

E.J. STRAIT, W.W. HEIDBRINK*, A.D. TURNBULL, M.S. CHU, H.H. DUONG*, **
General Atomics,
San Diego,
California, United States of America

ABSTRACT. The observed characteristics of toroidicity induced Alfvén eigenmodes (TAE) in DIII-D tokamak discharges are compared in detail with predictions of various theories of TAE mode stability, and good qualitative agreement is found. The observed range of unstable toroidal mode numbers ($n \sim 3$–6) is consistent with theoretical predictions. For DIII-D parameters, low mode numbers are damped by coupling to the stable Alfvén continuum, while high mode numbers are clamped by electron kinetic effects including coupling to kinetic Alfvén waves. A threshold for destabilization is observed experimentally at a fast ion beta of approximately 1%. The predicted driving and damping rates, estimated from experimental data, balance within about a factor of two for discharges at the threshold. It is demonstrated experimentally that the damping of TAE modes can be increased by current profile control, in this case with a peaked current profile produced by a negative current ramp, in qualitative agreement with theoretical predictions. A possible stabilizing effect of discharge elongation is also observed.

1. INTRODUCTION

Future fusion devices with significant amounts of alpha particle heating may be subject to instabilities driven by the free energy of the non-Maxwellian velocity distribution and non-uniform spatial distribution of the alpha particles. The toroidicity induced Alfvén eigenmode (TAE mode) is thought to be one of the most dangerous such instabilities, because the birth velocity of the alpha particles can be near the Alfvén velocity, allowing the mode to be driven resonantly. Once destabilized, the mode is expected to cause anomalous loss of the alpha particles, which could prevent ignition. The mode could also be destabilized by fast ions from high energy neutral beams injected for heating or non-inductive current drive. An understanding of the driving and damping mechanisms for this instability is essential in order to predict whether it in fact poses a threat to fusion reactors. This understanding can be gained from present experiments, in which the TAE mode can be studied by destabilizing it with fast ions produced by neutral beam injection.

The TAE mode has been observed experimentally in the DIII-D [1] and TFTR [2] tokamaks, where it is found to be capable of causing significant loss of fast ions. Loss of up to 70% of the beam power has been observed in DIII-D, in some cases with damage to optical components at the vacuum vessel wall, as well as large losses of non-resonant fusion products. These observations emphasize the importance of understanding this instability.

The TAE mode is a discrete mode which occurs in a gap in the continuous Alfvén wave spectrum. This gap is the result of toroidal coupling of shear Alfvén waves with toroidal mode number n and poloidal mode numbers m and $m + 1$. The existence of the TAE mode has been predicted by analytic theories in both the high n limit [3, 4] and the low n limit [5, 6]. Expressions have been derived for the alpha particle driving rate [6–8], and initial estimates of the instability threshold based on Landau damping associated with the electron curvature drift [6, 7] suggested that the mode could be destabilized at quite small values of the fast ion pressure. The threshold value of the fast ion beta, $\beta_f = p_f/(B^2/2\mu_0)$ (where p_f is the fast ion pressure and B the toroidal magnetic field) was found to be of the order of 10^{-3} to 10^{-5} in these initial estimates, significantly smaller than the experimentally observed threshold [1, 2] of $\beta_f \sim 10^{-2}$. However, subsequent theoretical work has shown that there are several other damping mechanisms, including ion Landau damping [8], coupling to the stable Alfvén wave continuum [9–11], and electron kinetic effects including coupling to kinetic Alfvén waves [12], which may account for the higher experimental threshold.

The TAE mode was found in independent experiments in DIII-D [1] and TFTR [2]. In the DIII-D experiments described in Ref. [1], modes with toroidal mode number $n \sim 2$–10 were observed, propagating

* University of California at Irvine, Irvine, California, United States of America.
** *Present address:* Princeton Plasma Physics Laboratory, Princeton, NJ, USA.

relative to the plasma in the direction of beam injection. The radial and poloidal mode structure, obtained from magnetic and soft X ray measurements, was consistent with a mode located in the vicinity of the $q = 3/2$ surface. The observed frequency was consistent with predictions of analytic theory for TAE modes, although a tendency was noted for the frequency to decrease below this value as beam power and beta increased. Fast ions were expelled during bursts of the instability, with up to 45% of the beam power being lost. Thresholds for destabilization were reported in the ratio of the parallel component of the fast ion speed to the Alfvén speed, $v_{\|0}/v_A \gtrsim 0.6$, and in the fast ion beta, $\beta_f \gtrsim 2\%$. In the more recent experiments reported here, the fast ion loss can be even larger (up to 70%) and the threshold in fast ion beta smaller ($\beta_f \gtrsim 1\%$).

Quite similar observations were reported in the TFTR experiment [2, 13]. Two apparent differences from DIII-D experiments were that the toroidal mode number of maximum amplitude tends to be higher in DIII-D (typically $n \sim 3$–5) than in TFTR ($n \sim 2$–3), and the threshold in fast ion beta is somewhat higher in DIII-D ($\beta_f \sim 1\%$) than in TFTR ($\beta_f \sim 0.5\%$). Possible reasons for these differences will be discussed.

The purpose of this paper is a detailed comparison of DIII-D experiments to theoretical predictions of the linear stability properties of TAE modes. Verification of theoretical damping rates of TAE modes is needed in order to be able to predict instability thresholds in alpha heated fusion devices with confidence. Our primary goal here is to gain insight into the scaling and relative importance of the various physical mechanisms which govern the behaviour of this instability. This understanding will provide guidance for further theoretical development and will also indicate ways in which these modes might be stabilized.

In this paper we report the first experiments aimed at controlling the stability of TAE modes, based on the predictions of the stability theories. These results indicate that it may be possible to mitigate or avoid the instability by control of the discharge profiles. In particular, the increased magnetic shear associated with a centrally peaked plasma current profile can increase the damping due to coupling to the stable Alfvén continuum, thus stabilizing the TAE mode.

In addition, we report the first experimental observations of the effect of discharge shaping on TAE mode stability. This is important since ITER and other future devices are expected to have highly non-circular cross-sections. Our results again should provide guidance for further theoretical development.

Only linear stability is considered here, which is sufficient to predict instability thresholds. Observations of TAE induced loss of fast ions [14, 15], leading to non-linear saturation of the instability [16], are discussed elsewhere.

This paper is organized as follows. In Section 2, we describe the experimental characteristics of the TAE mode, the tokamak discharges in which it occurs, the diagnostic measurements used in these experiments, and the equilibrium and stability calculations for which those measurements serve as input. In Section 3, we show that there exist thresholds for destabilization of the mode in several parameters related to the number and velocity of fast ions, in agreement with predictions for the TAE mode. In Section 4, we evaluate theories of the driving and damping rates for a marginally unstable case. For DIII-D parameters, we find that the damping is dominated at low mode numbers by continuum coupling, and at high mode numbers by coupling to kinetic Alfvén waves through electron kinetic effects. The continuum coupling, in particular, is sensitive to details of the current profile, suggesting that TAE modes might be controlled by modification of the current profile; in Section 5 we describe experiments which confirm this. The effects of variation in the discharge elongation are also described. Section 6 contains a final discussion, including suggestions for further experimental work and projections for future devices.

2. TECHNIQUES

The DIII-D tokamak [17] is well suited for TAE mode studies because of its capability of operation over a wide range of discharge shapes and conditions as well as its high neutral beam power density. The elongated, D shaped vacuum vessel and the versatile poloidal field coil set allow a wide range of plasma configurations.

In this section, a specific example of a DIII-D discharge with TAE modes will be used to illustrate the diagnostic measurements which are used in these experiments, and the methods of equilibrium reconstruction and stability analysis which are applied to these measurements. Discharge 71 524 which forms this example will also be used for much of the discussion of TAE mode stability in subsequent sections of the paper.

2.1. Observations of TAE modes

The primary diagnostic for detection of TAE modes in DIII-D consists of an extensive set of magnetic probes which are located inside the vacuum vessel and have a bandwidth of about 250 kHz. For the TAE mode experiments, typically 40 channels are digitized at a 500 kHz sampling rate, including an eight-channel toroidal array located near the outboard midplane and a 20-channel poloidal array. (Since the time of the experiments discussed here, additional probes with a bandwidth greater than 1 MHz have been installed.) Because of toroidal symmetry, the toroidal mode number of an oscillation can be obtained very reliably from the phase shifts between probes in the toroidal array. These probes have variable spacing down to a minimum of six degrees of toroidal angle, in principle allowing resolution of mode numbers $-30 < n < 30$. The location of these probes is shown later, in the discussion of diagnostics. Determination of the toroidal and poloidal mode numbers from the magnetic probe arrays is discussed further in Ref. [1]. The signal from one magnetic probe in the toroidal array is also high pass filtered, rectified, smoothed and sampled at a low rate to provide TAE amplitude data throughout the entire discharge. A low frequency cut-off of 90 kHz is selected as including most of the TAE activity with little or no contribution from harmonics of low frequency MHD activity.

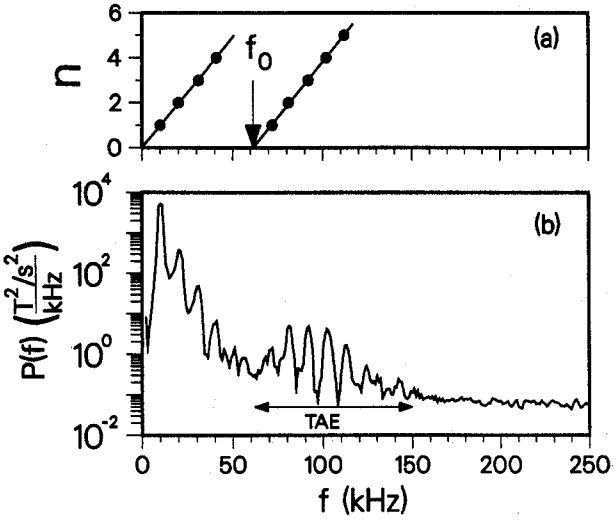

FIG. 1. (a) Toroidal mode number spectrum and (b) power spectrum for typical TAE activity, obtained from magnetic probes near the outboard midplane. f_0 is the inferred TAE mode frequency in the plasma rest frame. Discharge 71 524: B_T = 0.8 T, I_p = 0.6 MA, $\bar{n}_e = 3 \times 10^{19}\ m^{-3}$, P_{NB} = 5 MW.

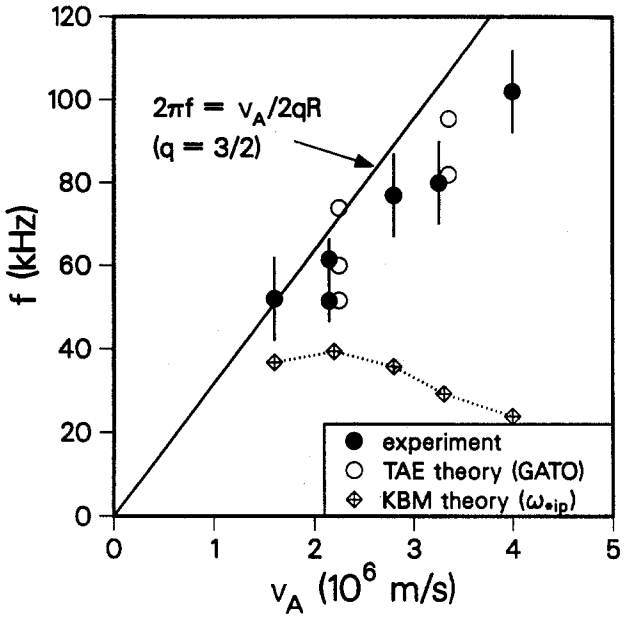

FIG. 2. Comparison of experimental and theoretical TAE frequencies versus Alfvén speed. Solid circles: measured (Doppler shift subtracted). Solid line: simple TAE theory ($\omega = V_A/2qR$, q = 1.5). Open circles: GATO calculation. Diamonds: kinetic ballooning mode prediction ($\omega_{*ip} = k_\theta \rho_i v_{ti} L_{pi}$). B_T = 0.6 to 1.4 T, I_p = 0.6 MA, $\bar{n}_e = 3 \times 10^{19}\ m^{-3}$, P_{NB} = 5 MW.

TAE modes have a distinctive signature in the Fourier spectrum of the magnetic probe data, as shown in Fig. 1. The usual low frequency MHD activity appears with frequencies $0 < f < 50$ kHz. The unusual feature in this spectrum is the prominent set of peaks between 70 and 150 kHz. The toroidal mode number n of the main spectral peaks, as obtained from the phase shifts of the toroidal magnetic probe array, is also shown. The toroidal rotation frequency f/n for the low frequency modes is comparable to that of the bulk plasma as measured from Doppler shifts of spectroscopic lines. The toroidal rotation frequency for the high frequency modes is significantly larger, indicating that these modes are propagating relative to the plasma as expected for Alfvén waves.

The measured frequency is an important piece of evidence for identifying the observed modes as TAE modes. Simple analytic theory for a TAE mode formed by the coupling of Alfvén modes with toroidal mode number n and poloidal mode numbers m and $m + 1$ gives the frequency as [6]

$$\omega = \frac{v_A}{2qR} \tag{1}$$

where $q = (m + 1/2)/n$, R is the major radius, and $v_A = B/\sqrt{\mu_0 \rho_m}$ is the Alfvén speed, with B the magnetic

field and ρ_m the mass density of the plasma. This dependence was tested by varying the toroidal field from 0.6 T to 1.4 T in a sequence of otherwise similar discharges. The plasma current was held fixed at 0.6 MA, the line averaged electron density at 3×10^{19} m^{-3}, and the neutral beam power at 5 MW. As seen in Fig. 2, the observed frequency increases linearly with the Alfvén speed and agrees well with the simple theoretical expression above if $q = 3/2$. The measured frequency plotted here has been corrected for the Doppler shift associated with toroidal rotation of the plasma, as discussed in Ref. [1]. In this plot, a representative Alfvén speed was estimated by using the line average density; discharge 71 524 corresponds to an Alfvén speed of $v_A = 2.2 \times 10^6$ m/s. The TAE frequency was calculated for two cases using the GATO code and complete equilibrium reconstructions, as described below. This more accurate theoretical prediction is also in good agreement with the observed frequency, as shown in Fig. 2. In both cases, multiple TAE modes at slightly different frequencies were found with GATO [18, 19]. The lower calculated frequencies agree well with the experimental values, while the predicted modes with higher frequencies are expected to be stabilized by coupling to the continuum near the edge of the discharge.

The very good agreement between the observed frequency and TAE mode theory is strong evidence that the observed modes are in fact TAE modes. Another possibility which was considered is that the observed modes might be kinetically destabilized ballooning modes [20], which could also be driven by the fast ions. A characteristic frequency for these modes is expected to be the ion diamagnetic drift frequency: $\omega \approx \omega_{*ip} = k_\theta \rho_i v_{ti} L_{pi}$, where k_θ is the poloidal wavenumber, ρ_i and v_{ti} are the gyroradius and thermal velocity of the thermal ions, and L_{pi} is the thermal ion pressure gradient scale length. This frequency is also plotted in Fig. 2, evaluated at the $q = 3/2$ surface, which coincides approximately with the maximum ion pressure gradient, and using $k_\theta = (3/2)\, n/r$, where n is the observed toroidal mode number with maximum amplitude. The drift frequency ω_{*ip} decreases slightly during the toroidal field scan, in disagreement with the observed frequency. This disagreement eliminates the possibility that the observed modes are kinetic ballooning modes.

2.2. Discharge parameters

Theories of the fast ion contribution to the growth rate of the TAE mode [6, 7, 8] show that destabilization requires $\omega_{*f}/\omega > 1$ and $v_f/v_A \gtrsim 1$, where ω_{*f} is the fast ion diamagnetic drift frequency, ω is the real frequency of the mode, v_f is the fast ion speed, and v_A is the Alfvén speed. The growth rate is maximized when the ratio v_f/v_A is near unity and the fast ion pressure gradient is large. (Weaker destabilization can also occur via a sideband resonance [8, 21, 22] when $v_f/v_A \gtrsim 1/3$.)

TAE modes can be strongly destabilized in DIII-D over a wide range of discharge configurations. The main restriction is that the toroidal field must be reduced from DIII-D's maximum of 2.1 T in order to reduce the Alfvén speed to a value near the fast ion speed: for a typical DIII-D case of 75 keV deuterium beams injected into a deuterium plasma with a density of 3×10^{19} m^{-3}, the Alfvén speed equals the injected fast ion speed when the toroidal field is 0.95 T. At high normalized beta ($\beta > 3\ I/aB$) some changes in TAE mode behaviour have been observed [19]. The present paper excludes this regime, which is discussed elsewhere [23]. In order to operate at low field and high power without encountering the MHD beta limit, regimes of good energy confinement such as the H mode must be avoided. The H mode is also undesirable for TAE mode experiments because the large density rise usually associated with the H mode would decrease the fast ion slowing down time, reducing the pressure of unthermalized fast ions. Since low density L mode limiter discharges allow the widest range and most reliable control of parameters such as β_f, ω_{*f}/ω, and v_f/v_A, they were chosen for the TAE mode experiments which will be discussed here.

The equilibrium flux surfaces for discharge 71 524 are shown in Fig. 3. The plasma has an elliptical cross-section with a modest elongation of $\kappa \sim 1.6$ and is limited on the graphite armour of the vacuum vessel's inner wall. The toroidal field B is 0.8 T, the plasma current I is 0.6 MA, and the safety factor q is 4.9 at the limiter flux surface. At this time in the discharge, 5 MW of deuterium neutral beams are injected into a deuterium plasma with a line-average density of 3×10^{19} m^{-3}. The volume averaged toroidal beta, β_T, is 3.5%.

Although the DIII-D neutral beam injector angles are fixed, half of the beams are quasi-tangential (with a tangency radius $R_{tan} = 1.10$ m), while the other half are quasi-perpendicular (with $R_{tan} = 0.74$ m). Only quasi-tangential beams were used for discharge 71 524 and the other cases discussed in detail in this paper, in order to maximize the parallel component of the fast ion speed. (The one exception is a case where quasi-perpendicular beams were used to determine the effect of varying the injection angle.)

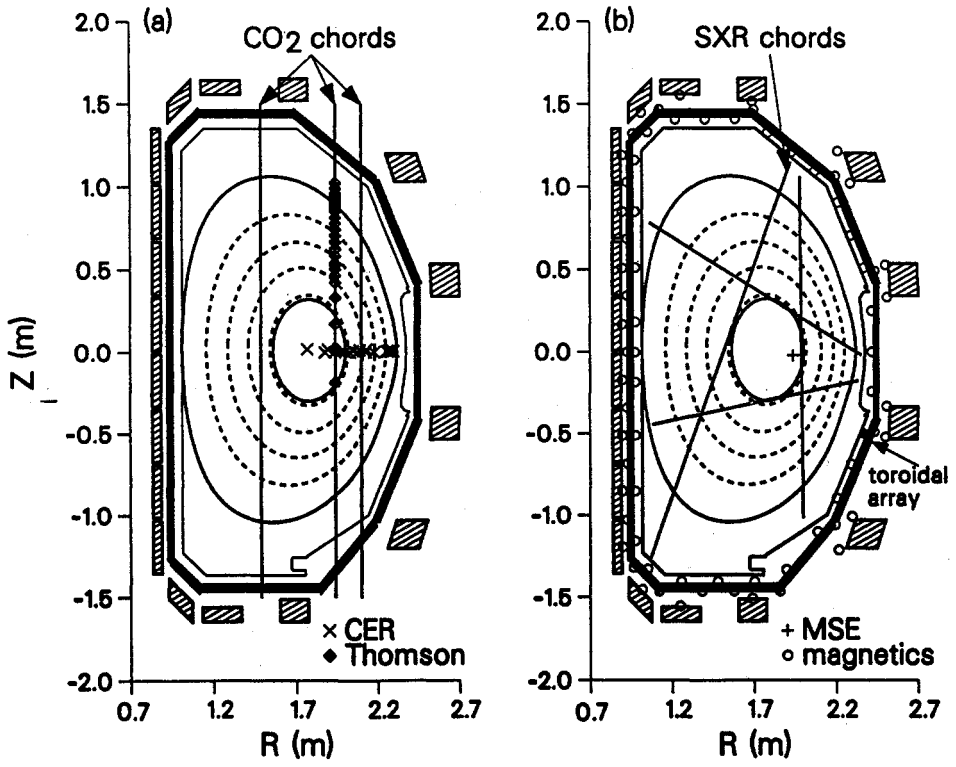

FIG. 3. Equilibrium flux surfaces and diagnostic measurement locations for discharge 71 524. The q = 1 surface and last closed surface are shown as solid lines. Also shown in cross-section are the poloidal field coils (shaded), vacuum vessel (heavy outline) and limiter surfaces. Diagnostic locations include (a) vertical CO_2 laser interferometer chords, and viewing points for charge exchange recombination (CER) and Thomson scattering, and (b) motional Stark effect (MSE) measurement point, soft X ray (SXR) chords corresponding to the sawtooth inversion, magnetic flux loops outside the vacuum vessel, and poloidal magnetic field probes inside the vessel. The poloidal location of the toroidal array of magnetic probes is indicated.

2.3. Equilibrium reconstruction and diagnostics

In order to evaluate the stability of TAE modes in an experimental discharge, the equilibrium must be known accurately. The EFIT code [24, 25] solves the Grad–Shafranov equilibrium equation to obtain a reconstruction of the equilibrium incorporating all available data: magnetic measurements as well as pressure and current profile measurements. Polynomial forms are used for the pressure and current profile related flux functions p' and ff'. It must be emphasized that these profiles are not fixed inputs provided to the code; rather, the coefficients of the polynomials are optimized to obtain the best simultaneous fit to all available data.

In the equilibrium reconstruction, magnetic data are obtained from 40 axisymmetric flux loops outside the vacuum vessel, and a poloidal array of 31 magnetic probes inside the vessel. The electron temperature profile is obtained from multipulse Nd-YAG laser Thomson scattering along a vertical path [26]. The electron density profile is obtained from Thomson scattering plus three vertical CO_2 laser interferometer chords. Ion temperature and toroidal rotation speed profiles are obtained from charge exchange recombination spectroscopy, utilizing one of the heating neutral beams [27]. The deuterium ion density is calculated from visible bremsstrahlung measurement of Z_{eff}, the measured electron density profile, and charge neutrality. Information about the current profile is obtained from a single-point motional Stark effect measurement of the pitch angle of the poloidal magnetic field [28], and from the location of the $q = 1$ surface as inferred from soft X ray observations of the sawtooth inversion radius. (Since the time of the experiments discussed here, the motional Stark effect diagnostic has been upgraded to 8 channels.) The locations of all of these measurements are shown in Fig. 3.

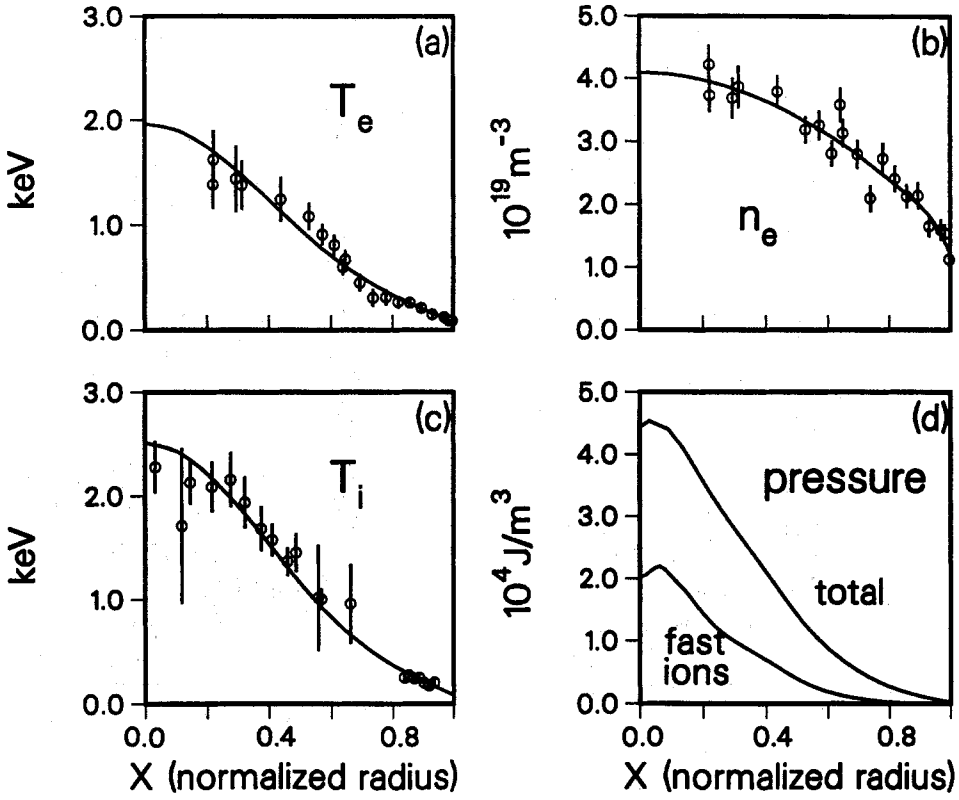

FIG. 4. Radial profiles for discharge 71 524: (a) T_e from Thomson scattering, (b) n_e from Thomson scattering and CO_2 interferometers, and (c) T_i from charge exchange recombination spectroscopy. Measured data points and cubic spline fit curves are shown. The total pressure profile (d) is calculated from the spline fits to the temperature and density profiles, and the classically calculated fast ion pressure profile (also shown).

The mass density is estimated from the electron density by assuming a mass to charge ratio $A/Z = 2$, which is valid for fully stripped light impurities as well as for the majority deuterium ions. Charge exchange recombination spectroscopy typically indicates a hydrogen concentration of less than 1% after an extended period of operation with deuterium, as was the case here. Spectroscopic data show that the dominant impurity in these discharges is carbon, as expected from the use of the inner wall's graphite armour as a limiter. The concentration of nickel, the most prevalent heavy impurity, is about two orders of magnitude smaller than the carbon concentration; therefore nickel can be neglected in the mass density.

The impurity density profile was calculated for discharge 71 524, using visible bremsstrahlung profile data and the measured electron density profile as input to a coronal equilibrium model in the ONETWO transport code [29]. Assuming that carbon is the only impurity, the calculation yields an average mass-to-charge ratio between 2.0 and 2.1 except in the outermost 10% of the minor radius, where it rises to about 2.5 at the edge of the plasma. Hence, with the square-root dependence of the Alfvén speed on the mass density, the assumption $A/Z = 2$ introduces only small errors which are restricted to the edge of the plasma.

The fast ion pressure profile is not measured directly, but instead is calculated by the ONETWO transport code [29], using the actual discharge geometry, density and temperature profiles, and neutral beam geometry, and assuming classical slowing down of the ions. In these low density discharges, the majority of the D-D fusion reactions are beam-target reactions, so the neutron emission as measured by scintillator detectors is proportional to the fast ion density. Anomalous loss of fast ions can be inferred from the neutron emission [1, 15], either by a comparison of the measured average emission to the classically predicted value or by the magnitude and repetition rate of the drops in neutron emission which occur during

bursts of TAE activity; these two methods generally agree well [15]. The fast ion pressure profile calculated from ONETWO is then reduced by the inferred anomalous loss.

Figure 4 shows the measured electron density, electron temperature, and ion temperature profile data used as input for the equilibrium reconstruction of discharge 71 524. Since the data are obtained at different locations and some measurements are line integrated, a spline fit is made of each profile as a function of a normalized flux co-ordinate. The poloidal flux is obtained from an initial equilibrium reconstruction using magnetic data only; in general, the magnetic flux geometry is found to change very little between this initial reconstruction and the final version using the measured profile data. These spline fits, along with the calculated fast ion pressure (also shown in Fig. 4), make up the actual profiles used as input to the EFIT code.

There is a large uncertainty in the fast ion pressure profile for these discharges. The classically calculated profile cannot be relied upon, because of anomalous loss of the fast ions in the presence of TAE modes. In the absence of a direct measurement, this difficulty can only be dealt with by considering a range of plausible fast ion pressure profiles in the equilibrium reconstruction. The pressure and safety factor profiles obtained for three such equilibria are shown in Fig. 5, along with the fast ion pressure inferred by subtracting the measured thermal pressure from the equilibrium pressure. In Case A, the equilibrium pressure profile was forced to follow closely the input pressure profile, including the classically calculated fast ion profile. In Case B, the central pressure profile was weighted less strongly in the equilibrium fit, resulting in a flatter fast ion profile. In Case C, $p'(\psi)$ was constrained to be small at the centre of the discharge, leading to a very flat fast ion profile. The total stored energy agrees equally well with diamagnetic loop measurements in all three cases. However, the fit to the other magnetic data (flux loops and magnetic probes) is best for Case B, and the major radius of the equilibrium $q = 1$ surface agrees best with the soft X ray sawtooth inversion radius in Case B. The flux surfaces shown in Fig. 3 are those of Case B.

2.4. Stability calculations

The reconstructed equilibrium is used as an input to several ideal MHD stability codes which calculate the

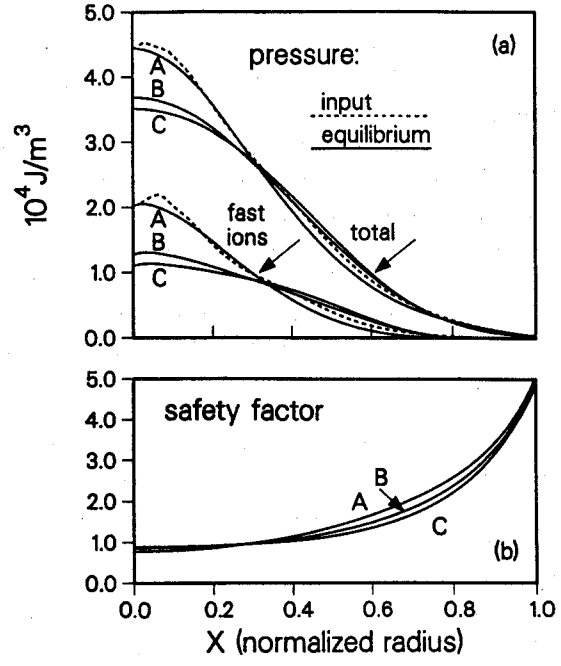

FIG. 5. Equilibrium profiles of (a) total pressure and fast ion pressure, and (b) safety factor from equilibrium fits for discharge 71 524. The input pressure profiles (dashed lines) are the same as in Fig. 4(d). Three possible equilibria, (A, B, and C) are shown.

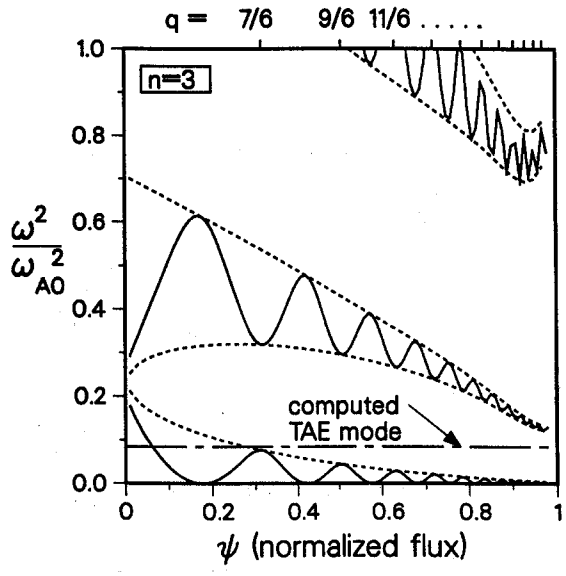

FIG. 6. Alfvén spectrum for discharge 71 524. The frequency is normalized to $\omega_{A0} = v_A/qR$ evaluated at the magnetic axis. Solid curves show the continuum spectrum for n = 3, and dotted curves show the envelope for the continua of all mode numbers, both calculated by CONT. The TAE frequency predicted by GATO is also shown.

gap structure of the Alfvén continuum, and the frequency and structure of TAE modes within the gap in the limits of high and low n. The codes discussed here do not incorporate kinetic effects or dissipation; so they are not capable of calculating growth and damping rates for the TAE modes. The equilibrium of Case B above is chosen for analysis here because it provides the best fit to magnetic and soft X ray data.

The structure of the shear Alfvén wave continuum spectrum is calculated with a modified version of the CONT code [5, 30]. The result is plotted in Fig. 6 for toroidal mode number $n = 3$, representative of the observed spectrum in Fig. 1. (In this example, acoustic wave coupling is omitted, i.e. incompressibility is assumed.) Several gaps in the Alfvén continuum spectrum are seen. The first gap at low frequency is caused by the coupling of Alfvén waves with poloidal mode numbers m and $m + 1$. It is in this gap that the TAE mode frequency is expected to appear. The large second gap at higher frequency is caused by the coupling of Alfvén waves with poloidal mode numbers m and $m + 2$, induced by the vertical elongation of the discharge. Ellipticity induced Alfvén eigenmodes (EAE modes) may exist in this gap. An envelope equation has been derived [30] for the gaps in the spectrum for all n, and this envelope is also shown.

The low n ideal MHD stability code GATO [31] has been modified to calculate stable ideal MHD eigenmodes. This code is used to find the real frequency and mode structure of TAE modes for the experimental equilibrium, in full toroidal geometry [18, 32]. The calculated frequency for a TAE mode with $n = 3$ is shown in Fig. 6, again with acoustic wave coupling omitted. The gaps associated with the various pairs of poloidal modes m and $m + 1$ are well enough aligned that the TAE mode frequency does not coincide with the continuum frequency (a possible source of damping), except possibly very near the centre of the discharge. As seen in Fig. 7, the eigenmode has a broad radial structure, with many poloidal harmonics. Several TAE modes are often found [18, 19], probably as a result of coupling of the single gap modes associated with different rational q surfaces [33].

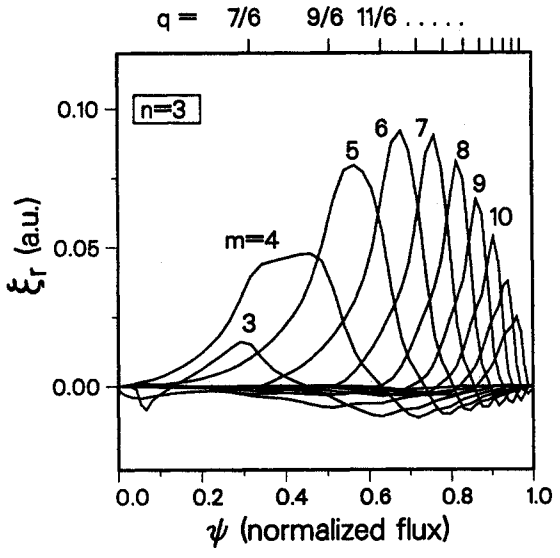

FIG. 7. Radial mode structure for a TAE mode in discharge 71 524, calculated by GATO. Amplitudes of the various poloidal harmonics are obtained from a spatial Fourier decomposition.

3. EXPERIMENTAL INSTABILITY THRESHOLDS AND SATURATION

The existence of the TAE mode has been demonstrated experimentally. The observation of large fast ion loss, discussed briefly below and in more detail in Ref. [15], shows that once it is destabilized the mode can have very undesirable consequences. In order to predict how to avoid the TAE mode in ITER or other burning plasma devices, the conditions for destabilization must be understood. In this section we shall describe the experimentally observed thresholds, and in the following section we shall compare these to theoretical predictions for the stability of the mode.

In order for a TAE mode to be destabilized by the free energy of the fast ion pressure gradient, two threshold conditions must be satisfied, as stated earlier. The first is a resonance condition: the fast ions must have the appropriate velocity to resonate with the Alfvén wave. That is, fast ions must be present with a velocity component $v_\parallel$ along the magnetic field comparable to the Alfvén speed v_A. The second is a stability condition: the gradient of the fast ion beta must be large enough to overcome the damping of the wave. The marginal stability condition provides a threshold criterion for β_f which depends on the physics of the damping mechanisms. The existence of thresholds in $v_\parallel/v_A$ and β_f has been demonstrated in a general way for a DIII-D database covering a wide range of discharge conditions [1], and an updated version of the threshold database will be shown here. In this section we shall also show examples of these thresholds in specific discharges and select a marginally stable case for analysis of the damping mechanisms. The fast ion loss caused by the TAE mode and the saturated amplitude of the mode will also be briefly discussed.

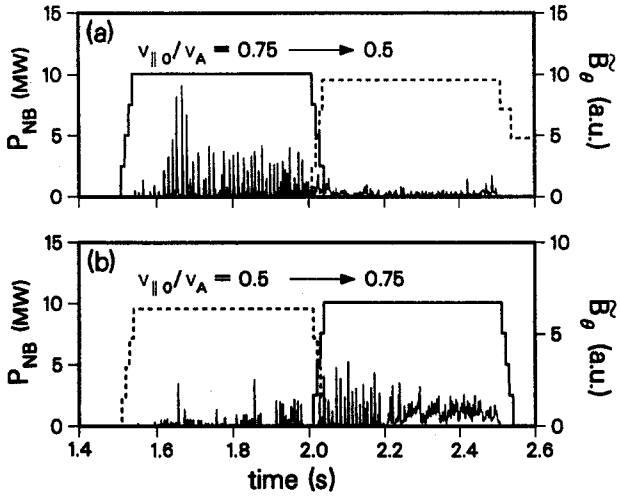

FIG. 8. Comparison of neutral beam injection angle, showing beam power and TAE activity (high pass filtered magnetic fluctuation amplitude, $\langle dB_\theta/dt \rangle$, 90 < f < 250 kHz). (a) Quasi-tangential beams (solid line) followed by quasi-perpendicular beams (dashed line). (b) Quasi-perpendicular beams followed by quasi-tangential beams. Discharges 71 497 and 71 498: B_T = 1.0 T, I_p = 0.6 MA, $\bar{n}_e = 3 \times 10^{19}$ m^{-3}.

The existence of a threshold in $v_\|/v_A$ implies that the stability of the observed mode should be sensitive to the angle of beam injection, and this is observed experimentally. An experiment was performed in which 10 MW of quasi-tangential beams were inejected for 500 ms, followed by 10 MW of quasi-perpendicular beams for another 500 ms. The discharge was then repeated with the order of the two sets of beams reversed. As shown in Fig. 8, in both discharges the TAE activity was much stronger during the quasi-tangential injection. The ratio of the parallel component of the initial fast ion velocity to the Alfvén speed is $v_{\|0}/v_A = 0.5$ for the quasi-perpendicular case and $v_{\|0}/v_A = 0.75$ for the quasi-tangential case, suggesting that the threshold lies between these values. Here, $v_{\|0}$ is evaluated at the magnetic axis for the nominal tangency radius of injection, and v_A is estimated by using the line averaged density $\bar{n}_e$ and the vacuum toroidal field at the magnetic axis. For all other experiments discussed in this paper, only quasi-tangential beams were used in order to drive the TAE modes as strongly as possible. The threshold in $v_{\|0}/v_A$ found by varying v_A at fixed $v_{\|0}$ agrees with the preceding results, as will be discussed in more detail in Section 4.

There are several possible explanations for the fact that the observed threshold value $v_{\|0}/v_A \gtrsim 0.6$ is below the expected value of unity. Pitch angle scattering tends to isotropize the fast ions, creating a tail on the distribution with $v_\|$ up to the birth velocity v_0 of the fast ions [1]. The observed threshold in terms of v_0 is $v_0/v_A \gtrsim 0.9$ for the quasi-tangential beams. Notice also that the actual frequency of the mode, from both experimental measurements and calculations with the GATO code, is 10% to 20% lower than predicted by simple theory. This suggests that in the resonance condition rewritten as $v_\| = \omega/k_\|$, the value of ω on the righthand side should be reduced by 10% to 20% from the simple estimates used here, bringing the two sides into closer agreement. Furthermore, a contribution is expected from the sideband resonance [8, 21, 22], which requires only $v_0/v_A > 1/3$. Finite fast ion orbit width effects [34] may enhance the driving rate for $1/3 < v_0/v_A < 1$.

It has also recently been shown that trapped ions may drive TAE modes by resonance with their precessional drift [21, 34], in which case the criterion $v_{\|0} \gtrsim v_A$ of course does not apply. Experiments in TFTR have shown that TAE modes can be destabilized by a population of trapped ions created with ICRF heating [35]. The driving rates may be comparable for the same pressures of circulating or trapped fast ions. However, Monte Carlo calculations show that for quasi-tangential injection in DIII-D, a large majority of the fast ions are born on circulating orbits [36], so we do not expect trapped ions to play a large role in the present experiments.

The second anticipated threshold condition, the stability condition for the fast ion pressure, can be observed in a scan of the neutral beam power. For the example of discharge 71 524 presented here, the beam

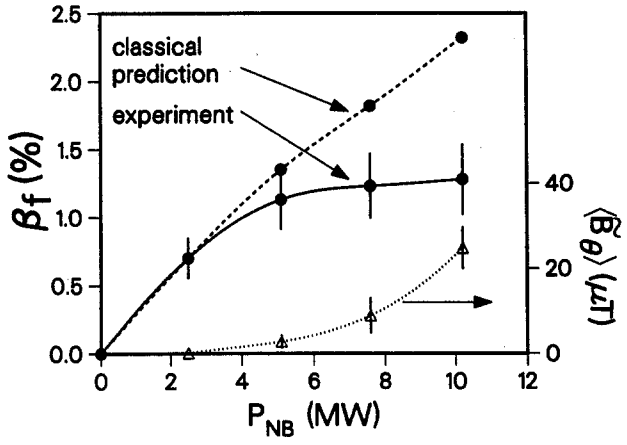

FIG. 9. Dependence of TAE activity on neutral beam power in discharge 71 524. The fast ion beta predicted by using classical slowing down (dashed line) is compared to the experimental value inferred from neutron emission (solid line). The time averaged TAE amplitude at the outboard wall (dotted line) is also shown.

power was increased in steps of 2.5 MW during a single discharge. The duration at each power level was several times the fast ion slowing down time and the thermal energy confinement time, allowing a thermal equilibrium to be approached. As seen in Fig. 9, the TAE amplitude increases rapidly when the power exceeds about 5 MW and the fast ion beta exceeds about 1%. (The threshold case at 5 MW will be used for a more detailed analysis in Section 4 below.) The fast ion beta predicted by the classical slowing down calculation in the ONETWO code increases approximately linearly with the beam power. However, as the TAE amplitude increases, the anomalous fast ion loss estimated from the neutron emission also increases, up to a loss of almost half of the fast ions at 10 MW of input power. The net fast ion beta, estimated by subtracting the anomalous loss from the classical prediction, saturates at $\beta_f \approx 1.2\%$. It should be noted that this estimate also includes fast ion loss from other causes (e.g. fishbone instabilities); the largest fast ion loss may occur from the simultaneous action of fishbones and TAE modes [15].

The strong saturation of fast ion beta seen in Fig. 9 is consistent with the expectation that fast ion loss induced by the TAE mode is the primary mechanism for non-linear saturation of the mode [16, 37]. The fast ion loss [15] and non-linear saturation [16] are discussed elsewhere, but we will note the following points. The TAE activity is sometimes observed as large amplitude bursts lasting only a few cycles and sometimes as a nearly continuous oscillation; a mechanism has been proposed for the non-linear saturation of the mode which includes both types of behaviour [38]. In the present examples, under conditions of a large, nearly continuous oscillation and saturated fast ion beta, the peak amplitude measured by magnetic probes at the outer wall can be as large as $\delta B_\theta/B \sim 10^{-4}$. GATO calculations show that δB_θ is about an order of magnitude larger at its peak in the plasma than at the edge, while δB_r is somewhat smaller than δB_θ, consistent with $k \cdot \delta B = 0$. Then the perturbation in the plasma is roughly $\delta B_r/B \sim 5 \times 10^{-4}$ which is near the predicted threshold $\delta B_r/B \sim 10^{-3}$ for stochastic orbits and large fast ion loss [39].

A more general determination of the thresholds for destabilization of TAE modes has been obtained from an examination of all DIII-D discharges with a sufficiently high sampling rate for the magnetic data (Nyquist frequency $\geq$250 kHz). In this study the 'classical' fast ion beta was estimated from the beam power, stored energy, and $\bar{n}_e$, on the assumption of classical slowing down; comparison of this estimate with ONETWO calculations for several discharges shows that the typical error in the estimated fast ion beta is ~25%. For the unstable cases, fast ion losses can reduce the actual fast ion beta by more than 50% from the classical estimate, but the losses are negligible for most of the stable conditions.

The results, shown in Fig. 10, indicate that TAE modes are usually unstable in plasmas that have intense populations of fast ions with $v_f \simeq v_A$. The instability is present but generally weaker for $0.7 \lesssim v_f/v_A \lesssim 1$. The threshold in fast ion beta is about $\beta_f \sim 1\%$, although there are a few marginally unstable cases with smaller β_f. Instability is observed over a very wide range in parameter space, including currents between 0.4 and 1.2 MA, toroidal fields between 0.7 and 1.4 T, edge safety factors between 2.0 and 7.7, densities between 2.0 and 5.6×10^{19} m^{-3}, and beam powers between 2 and 19 MW. TAE modes occur in nearly circular ($\kappa = 1.1$) and highly elongated ($\kappa = 2.2$) plasmas, in both limiter and divertor configurations, and in both L mode and H mode discharges. They have not been observed for $v_f/v_A > 1.6$, for $\beta_f < 0.4\%$, for low normalized beta ($\beta_N = \beta/(I/aB) < 1.6$), or during

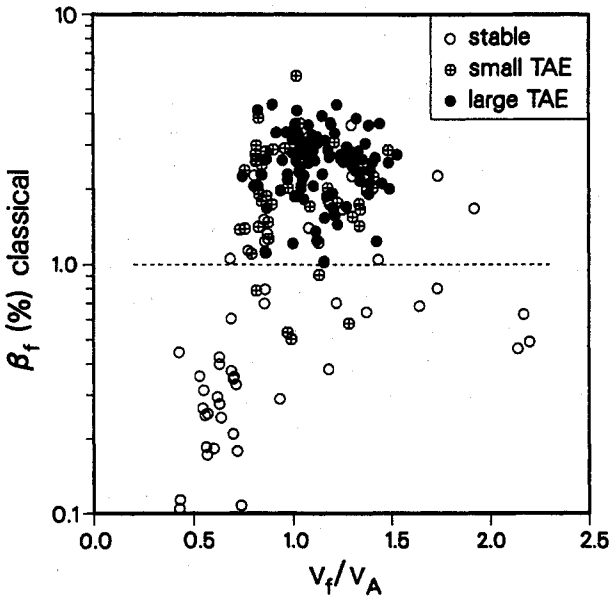

FIG. 10. Range of observed TAE instability in the DIII-D database, shown versus the classically estimated fast ion beta β_{fc} and the ratio of injected fast ion speed to the Alfvén speed. The data include both deuterium and hydrogen injection (P_{NB} = 2 to 19 MW) into both divertor and limiter discharges with B_T = 0.6 to 2.2 T, I_p = 0.4 to 1.6 MA, $\bar{n}_e$ = 2.0 to 8.4 × 10^{19} m^{-3}, q_{95} = 2.0 to 7.7, κ = 1.1 to 2.2, dI_p/dt = −4.1 to 1.4 MA/s, and β_N = 0.4 to 6.4.

hydrogen beam injection. The absence of TAE modes at low β_N is a consequence of the requirements of high beam power and low toroidal field (to achieve $v_f/v_A \sim 1$) which together tend to produce high β_N plasmas, while their absence during hydrogen beam injection is probably a result of the shorter slowing down time for the beam ions, leading to a smaller fast ion beta.

4. COMPARISON WITH LINEAR GROWTH RATE THEORIES

In this section we compare the observed characteristics of TAE modes against published theories for the linear driving and damping rates. The main purpose here is to gain insight into the scaling and relative importance of the various physical mechanisms which govern the behaviour of this instability. This understanding will show which theories should be emphasized in future work and will allow us to begin to consider how to control or avoid the instability.

In the present state of theory and experimental analysis, we cannot hope to make an accurate, quantitative comparison of all theories for the experimental discharges. To date much of the theoretical work on growth rates (and all theories to be discussed in this section) have employed the simplifying assumptions of large aspect ratio, low beta, and a circular cross-section; clearly these approximations are not good for the DIII-D discharges studied here. Additional simplifying assumptions will also be mentioned below. Furthermore, as discussed above in Section 2.3, there is some uncertainty in the experimental fast ion pressure profile. Therefore it must be understood that, when these theories are discussed here in connection with DIII-D data, the quantitative values are not to be taken too seriously. Nevertheless, the results should be qualitatively meaningful.

In this analysis the plasma is modelled in one dimension. All theories applied in this section are local theories. That is, the TAE mode is assumed to be radially localized (despite the GATO calculations shown in Fig. 7, for example, which indicate a rather broad radial structure) so that the theoretical expressions are evaluated by using only the local values of the experimental profiles and their gradients. Profiles of density, temperature, safety factor, etc. are obtained from equilibrium reconstructions with complete profile data, as discussed in Section 2. Gradients are evaluated along the minor radius r at the midplane, on the outboard side of the magnetic axis, since this is the location of largest mode amplitude.

The fast ions drive the mode resonantly and may also contribute to Landau damping. Several similar expressions have been derived for the fast ion driving rate [6–8]. We have chosen to use Eq. (69) of Ref. [8], which uses a slowing down velocity distribution and incorporates the $v_A/3$ sideband term:

$$\frac{\gamma_f}{\omega} = q^2\beta_f \left\{ nq \left(\frac{2}{3}\right) \frac{\rho_{\theta f}}{L_{pf}} \left[h_s(x_f) + \frac{1}{3} h_s\left(\frac{x_f}{3}\right) \right] - \left[g_s(x_f) + g_s\left(\frac{x_f}{3}\right) \right] \right\} (1 + k_\theta \rho_f)^{-1} \quad (2)$$

Here, γ_f is the growth rate due to the fast ions, ω is the real frequency of the mode, n is the toroidal mode number, q is the safety factor of the resonant flux surface, $x_f = v_A/v_f$ where v_f is the initial velocity of the fast ions, $\rho_{\theta f}$ is the poloidal gyroradius of the fast ions, and $L_{pf} = -p_f(dp_f/dr)^{-1}$ is the fast ion pressure gradient scale length. Integrals over the slowing-down distribution are expressed by $h_s(x) = (3\pi/16)(1 + 6x^2 - 4x^3 - 3x^4) H(1 - x)$ and $g_s(x) = (3\pi/16)x(3 + 4x - 6x^2 - x^4) H(1 - x)$, where H is the Heaviside step function. Landau damping by the magnetic curvature drift of the fast ions is also included in Eq. (2). The fast ion velocity distribution is assumed to be isotropic, which may be a poor approximation for beam heated discharges.

Equation (2) includes a finite Larmor radius term for the fast ions which was not present in Ref. [8]. At high mode numbers, the poloidal wavelength of the mode may approach the fast ion gyroradius, weakening the wave–particle interaction. The right hand side of Eq. (2) includes an approximate correction for FLR effects [40] through the factor $(1 + k_\theta \rho_f)^{-1}$, where $k_\theta = m/r$ is the poloidal wavenumber and ρ_f is the fast ion gyroradius. Then with the leading terms $nq\,\rho_{\theta f} \propto k_\theta \rho_f$, the expression for γ_f increases linearly with mode number for $k_\theta \rho_f \ll 1$, and saturates for $k_\theta \rho_f \gtrsim 1$. It has been suggested that the radial width Δ_m of the TAE mode may become narrower than the radial excursion $\Delta_b = q\rho_f$ of the drift orbits of passing ions, leading to a factor $\Delta_m/\Delta_b \sim (k_r \rho_f)^{-1}$ reduction in the driving term [41]. Recent numerical calculations [34] suggest that finite orbit width effects become important at $k_\theta \rho_f > 1$. However, GATO calculations and experimental measurements [1] indicate that the mode structure is broad with many poloidal harmonics. Therefore we use an estimate of the radial width consistent with an extended mode structure formed by coupling of several TAE modes at neighbouring rational surfaces [33], $\Delta_m/r = \hat{\epsilon}/s$, where $\hat{\epsilon} = \sigma\epsilon s/s_A$, $\sigma = 5/2$, ϵ is the inverse aspect ratio of the flux surface,

$s = (r/q)\,(\mathrm{d}q/\mathrm{d}r)$ is the magnetic shear, and $s_A = (r/\omega_A)(\mathrm{d}\omega_A/\mathrm{d}r)$ is the shear in the Alfvén frequency $\omega_A = v_A/qR$. With this definition, in most cases $\Delta_m > \Delta_b$; therefore the radial orbit width correction is omitted in Eq. (2).

The presence of a background thermal plasma leads to Landau damping of a propagating wave. Several similar expressions have been derived for Landau damping of the TAE mode [6–8]. We have chosen to use Eq. (66) of Ref. [8], for consistency with the fast ion driving term, and because it includes the $v_A/3$ sideband term:

$$\frac{\gamma_e}{\omega} = -q^2\beta_e\left[g_m(x_e) + g_m\left(\frac{x_e}{3}\right)\right] \tag{3}$$

$$\frac{\gamma_i}{\omega} = -q^2\beta_i\left[g_m(x_i) + g_m\left(\frac{x_i}{3}\right)\right] \tag{4}$$

Here γ_e and γ_i are the Landau damping rates due to magnetic curvature drift of the thermal electrons and ions, with $x_e = v_A/v_e$ and $x_i = v_A/v_i$, where v_e and v_i are the electron and ion thermal velocities. Integrals over the Maxwellian distributions are expressed by $g_m(x) = (\pi^{1/2}/2)\,x(1 + 2x^2 + 2x^4)\,e^{-x^2}$. For typical tokamak parameters and moderately low mode numbers as observed in this experiment, Landau damping due to electron parallel motion is small compared to the curvature drift contribution [42].

Coupling to the stable Alfvén wave continuum is a potentially important damping mechanism. Theoretical expressions have been developed for continuum damping in the high n limit [9, 10] and the low n limit [11]. Some progress has also been made in numerical calculations for more realistic discharge geometries [43–46]. We have chosen to use Eq. (13) of Ref. [10], which can be applied for arbitrary values of the magnetic shear:

$$\frac{\gamma_c}{\omega} = -\frac{\sigma\epsilon}{2}\left(\frac{1}{g_0(s)} + \frac{1}{g_\infty(s)}\right)^{-1} \tag{5}$$

with

$$g_\infty(s) = \frac{G(s)}{(m\hat{\epsilon})^{3/2}}\left[\exp(-m\hat{\epsilon}H_+(s)) + \exp(-m\hat{\epsilon}H_-(s))\right] \tag{6}$$

where γ_c is the continuum damping rate, and s and $\hat{\epsilon}$ have been defined above. Numerical values for $g_0(s)$, $G(s)$, $H_+(s)$, and $H_-(s)$ are taken from Table I of Ref. [10], along with asymptotic expressions for the limits of high and low shear. The functions $g_0(s)$ and $g_\infty(s)$ are asymptotic values for low and high $m\hat{\epsilon}$, respectively, representing the limiting cases of a single TAE mode and the coupling of several adjacent TAE modes. It should again be noted that this is essentially a local theory and may not be a good approximation for DIII-D discharges. For example, with the proper choice of profiles the TAE frequency could fail to intersect the continuum, resulting in little or no continuum damping. Such a case is discussed in Section 5.1 below.

A non-perturbative kinetic analysis of electron parallel dynamics has been developed [12], including such non-ideal effects as collisions, trapped electrons, and coupling to kinetic Alfvén waves. The predicted damping rate can be much larger than for collisionless Landau damping, primarily because of the kinetic Alfvén wave coupling. A somewhat smaller damping rate is obtained from a theory which includes only trapped electron collisions [47].

We use the analytic form given in Eq. (42) of Ref. [12]:

$$\frac{\gamma_k}{\omega} = -3\left[\frac{m(m+1)}{2m+1}\left(\frac{s}{2^{1/2}}\right)\frac{\rho_s}{r}\right]^{2/3} \tag{7}$$

where γ_k is the damping due to electron kinetic effects, and ρ_s is the ion gyroradius evaluated at the electron thermal speed. This expression is valid when $8s^2(2\epsilon)^{-3}(\rho_s/r)^2\,[m(m+1)]^{1/2}\,(2m+1) \gtrsim 1$, which is satisfied in the DIII-D examples for $m \gtrsim 2$–3.

These expressions can now be evaluated by using experimental data and can be compared with the observed thresholds. The resonance threshold condition is expressed as $\gamma_f > 0$, while the stability threshold condition is $\gamma_f + \gamma_e + \gamma_i + \gamma_c + \gamma_k > 0$.

A comparison of the calculated resonance condition with the observed threshold in v_f/v_A is shown in Fig. 11. Here v_A was varied by changing the toroidal field with plasma current, density, and beam power held constant; the data come from the toroidal field scan discussed in Section 2. In Fig. 11(a) the fast ion driving rate γ_f given in Eq. (2) is evaluated by using p_f, $p_{\theta f}$, and L_{pf} at the $q = 3/2$ surface in discharge 71 524 with 5 MW injected, with a typical experimental value $n = 4$ for the toroidal mode number. The parameters β_f and v_f/v_A are then scaled appropriately to model a scan of the toroidal field, while p_f, $\rho_{\theta f}$, and L_{pf} are held fixed as expected for constant beam power, density and plasma current. The two thresholds at $v_f = v_A/3$ and $v_f = v_A$ are seen. The observed TAE mode amplitude is plotted versus v_f/v_A, consistent with the assumption of an isotropic fast ion velocity distribution. As seen in Fig. 11(b), the observed amplitude is qualitatively consistent with the calculated fast ion driving rate, including the small but non-zero amplitude at $1/3 < v_f/v_A < 1$, the increase by an order of magnitude at $v_f/v_A \sim 1$, and the saturation at high v_f/v_A.

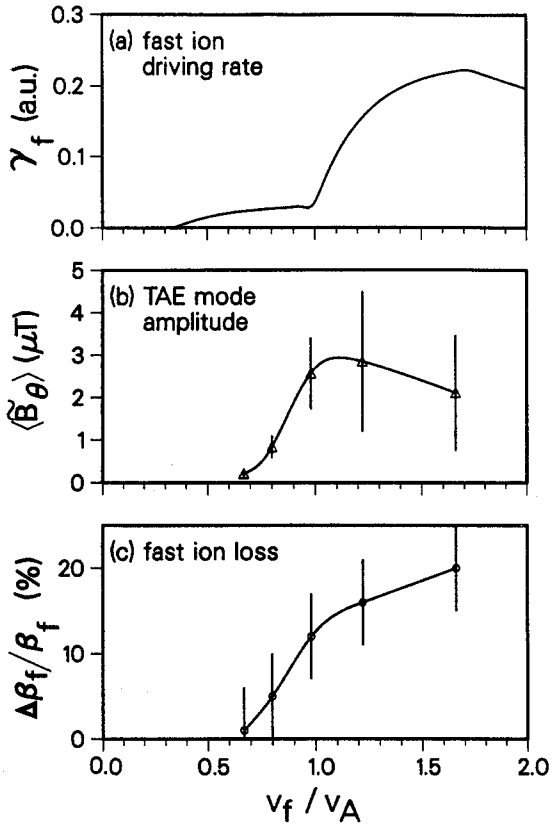

FIG. 11. Comparison of predicted and measured threshold in v_0/v_A, the ratio of injected fast ion speed to the Alfvén speed. (a) Predicted fast ion driving rate, estimated for n = 4 *at* q = 3/2 *in discharge 71 524 and scaled with varying* B_T. *(b) Time averaged TAE amplitude at the outboard wall from Fourier analysis of magnetic probe signals. (c) Proportion of fast ions lost due to MHD activity, estimated from neutron emission. The discharges are the same scan of the toroidal field shown in Fig. 2.*

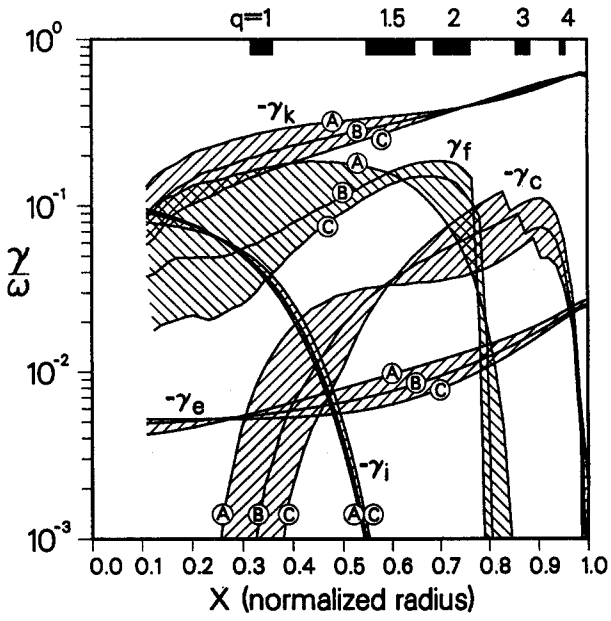

FIG. 12. Radial profiles of predicted contributions to the TAE mode growth rate γ/ω, evaluated for n = 4 *in discharge 71 524. γ_f: fast ion drive, $-\gamma_e$ and $-\gamma_i$: electron and ion Landau damping, $-\gamma_c$: continuum damping, $-\gamma_k$: electron kinetic damping. The shaded bands represent the profile variation between the three equilibrium cases (A, B, C) shown in Fig. 5; the solid bars at the top represent the variation in the positions of rational* q *surfaces.*

The anomalous fast ion loss inferred from the neutron emission, shown in Fig. 11(c), is well correlated with the TAE mode amplitude and also increases by about an order of magnitude as v_f/v_A increases above unity.

In order to understand the stability threshold, the expressions for the various contributions to the growth rate of the TAE mode are plotted in Fig. 12 for the slightly unstable case corresponding to the 5 MW phase of discharge 71 524 (see Fig. 9). A typical experimental value $n = 4$ is again chosen for the toroidal mode number. Results are shown for the three pressure profile cases discussed in Section 2.3. The differences in the p and p_f profiles lead to large differences in the γ_f profile and to smaller differences in γ_c and γ_k through the magnetic shear.

In this figure, each growth rate term is evaluated and plotted as a continuous function across the minor radius of the plasma. For a given value of n, the poloidal mode number is treated as a continuous variable: $m(r) = nq(r) - 1/2$. Since these expressions are taken from local theories, they should be interpreted as applying to a localized TAE mode at each radial location. Although the results are plotted as continuous curves, it must be kept in mind that TAE modes are associated only with integer values of m, corresponding to discrete values of $q = (m + 1/2)/n$. While the radial structure of the TAE mode has proved difficult to measure experimentally in DIII-D, both GATO calculations [18, 19] and soft X ray measurements [1] indicate that the mode amplitude is peaked near the $q = 3/2$ surface. A comparison of the inferred Doppler shift of the mode [1] with the measured toroidal rotation velocity profile is consistent with a radial location between $q = 1$ and $q = 3/2$. Therefore the region $1 < q < 2$ is of greatest interest for the estimation of driving and damping rates.

The relative importance of the various terms can be easily seen in Fig. 12. (Note the logarithmic scale of the ordinate.) Electron Landau damping is very small, rising only at the edge where the electron temperature is very low. The $v_A/3$ sideband term allows a significant contribution from ion Landau damping in the region of high ion temperature near the centre of the discharge. Continuum damping rises rapidly with minor radius as ϵ and shear increase. The fast ion driving term drops rapidly at $q \gtrsim 2$, as the fast ion pressure gradient becomes small. Over much of the region $1 < q < 2$, where the mode amplitude is expected to be largest, the fast ion driving rate is much larger than either the Landau damping or the continuum damping rate. Only the electron kinetic damping rate is large enough to match or exceed the fast ion drive. These qualitative conclusions hold for all three pressure profile cases.

The fast ion driving rate γ_f and the total damping rate, essentially equal to $-\gamma_k$ for $n = 4$, balance within about a factor of two, with experiment being somewhat more unstable than predicted. This agreement is quite good, given that the theories are not strictly applicable to the experimental configuration. Furthermore, in one model case, a more exact numerical calculation gave a value for γ_k about a factor of two smaller than the analytic expression [12]. If the same ratio applies to the DIII-D discharge considered here, then $-\gamma_k$ would agree more closely with γ_f. However, because of the many approximations and uncertainties in applying these theoretical expressions, the general trends and orders of magnitude must be considered more significant than precise numerical agreement.

The observed range of mode numbers is consistent with the predicted dependence of the driving and damping terms on the mode number. The fast ion driving rate increases with the mode number (neglecting the fast ion Landau damping contribution) until the FLR term causes it to saturate: thus $\gamma_f \propto n$ at low n, and $\gamma_f \sim$ const at high n. The ion and electron Landau damping rates $-\gamma_i$ and $-\gamma_e$ are independent of n, the continuum damping rate decreases with n approximately as $-\gamma_c \propto n^{-3/2}$, while the electron kinetic damping increases with n approximately as $-\gamma_k \propto n^{2/3}$. These trends are illustrated in Fig. 13, where the various γ's are evaluated at the $q = 3/2$ surface using the pressure profile of Case B. (The $q = 3/2$ surface is chosen as representative, because GATO calculations show the largest mode amplitude in this vicinity.) Continuum damping cuts off the low mode numbers, while electron kinetic damping is the only mechanism which can account for the cut-off of high mode numbers. The total predicted growth rate $\gamma = \gamma_f + \gamma_e + \gamma_i + \gamma_c + \gamma_k$, shown in Fig. 14, never exceeds zero due to the uncertainties in applying the theories to DIII-D experimental cases. Nevertheless, the most unstable mode numbers lie in a broad range of $2 \lesssim n \lesssim 5$, in good agreement with experimental observations (Fig. 1, for example).

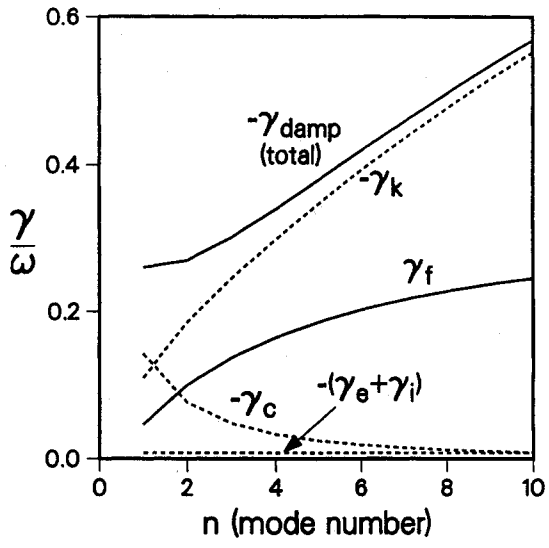

FIG. 13. Mode number dependence of predicted contributions to the TAE mode growth rate γ/ω, evaluated at q = 3/2 in discharge 71 524. Solid lines: γ_f: fast ion drive, $-\gamma_{damp} = -(\gamma_k + \gamma_c + \gamma_i + \gamma_e)$: total damping rate. Dashed lines: $-\gamma_k$: electron kinetic damping, $-\gamma_c$: continuum damping, $-(\gamma_e + \gamma_i)$: sum of electron and ion Landau damping.

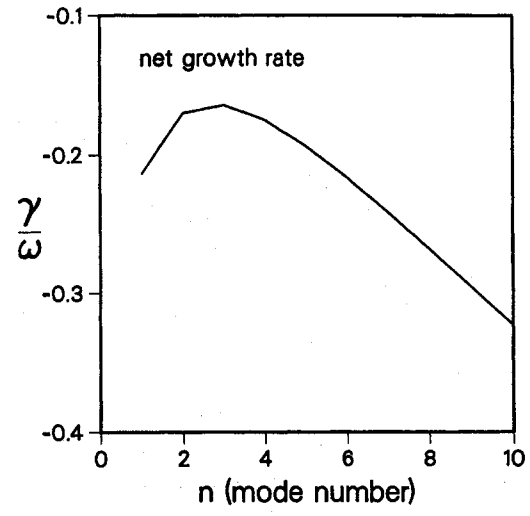

FIG. 14. Mode number dependence of predicted net growth rate $\gamma = \gamma_f + \gamma_{damp}$, evaluated at q = 3/2 in discharge 71 524.

A similar analysis of twelve other discharges with observed TAE instabilities has yielded results which are qualitatively consistent with those described above. These discharges were chosen to represent a wide range of plasma configurations, including limiter L mode discharges with elongations from 1.2 to 1.6, and double null divertor H mode discharges with elongations up to 2.1. For a toroidal mode number $n = 4$, electron kinetic damping always dominates at the $q = 1.5$ surface. There can be a significant contribution from ion Landau damping in the centre of the discharge, while continuum damping makes a significant contribution at larger minor radius. The ratio of the fast ion driving rate (estimated from the neutron emission) to the damping rate is found to range from about one half to unity. This is reasonable agreement considering the uncertainties in estimating the fast ion pressure profile and the limitations of the theoretical expressions used here, and is consistent with the hypothesis that mode induced losses limit the fast ion pressure at the marginally stable value.

We conclude that there is reasonably good agreement between theories of TAE growth rate and experimental observations in DIII-D. At marginal stability the predicted driving and damping rates agree within a factor of two. That is, the theoretically estimated threshold in fast ion beta is only about a factor of two larger than the experimental value. Continuum damping dominates for low mode numbers, while electron kinetic damping dominates for high mode numbers. With a doubling of the ion temperature, ion Landau damping could also become important in the centre of the discharge, particularly for low mode numbers. Collisionless electron Landau damping is negligible in comparison with the other damping mechanisms. An intermediate range of mode numbers is predicted to be most unstable, in agreement with the experimental observations. These conclusions are insensitive to the choice of equilibrium pressure profile, as long as consistency is maintained with the measured thermal pressure profile, neutron emission, and magnetic data. The conclusions are also insensitive to the radial location of the mode, within the range $1 < q < 2$.

5. CONTROL OF TAE MODES

The understanding of the damping mechanisms for TAE modes which was gained in the preceding section can point the way toward stabilization of these modes by control of the background thermal plasma.

The simplest means of avoiding TAE modes, of course, would be to decrease the fast ion driving term. The resonance condition can be avoided by reducing v_f/v_A, or the growth rate can be reduced by decreasing the fast ion beta or increasing the fast ion pressure gradient scale length. However, we must assume that in a fusion reactor, these quantities are dictated largely by such considerations as magnet technology and the alpha particle power density required for ignition, and are not easily subject to change.

In this section we shall describe a preliminary experiment in which TAE modes were transiently suppressed by altering the current density profile in the plasma. The influence of discharge elongation will also be discussed.

5.1. Current profile control

Current profile control is a promising approach for suppression of TAE modes, since both the continuum damping and electron kinetic damping terms depend on the magnetic shear s. In the analytic approximation, electron kinetic damping increases with shear as $\gamma_k \sim s^{2/3}$. The continuum damping rate γ_c has a more complex functional dependence on the shear, but the dependence is strong, at least linear for $s \gtrsim 1$, and becoming much stronger for $s < 1$. Therefore we expect that increasing the magnetic shear should increase the damping. Furthermore, increasing the shear should preferentially damp the lower mode numbers since the dependence on shear is stronger for continuum damping and this mechanism is most important for low mode numbers.

TAE modes can be stabilized temporarily with a transient modification of the current profile produced by ramping the plasma current. Figure 15 shows time traces for discharge 71 531, in which the current was ramped down rapidly from 0.9 to 0.6 MA. A reference case with constant plasma current at the lower value, discharge 71 517, is also shown. After the end of the current ramp, the values of beam power, plasma current, safety factor and electron density are the same in the two discharges. The current ramp-down in discharge 71 531 results in a peaked current profile with high shear, which then relaxes on a slower time-scale toward a steady state profile. An indication of the change in the current profile is given by the internal inductance ℓ_i (calculated from equilibrium fits by using magnetic data only), which is high at the end of the current ramp and then decays toward the lower value of the constant current discharge. More detailed equilibrium fits show that the peaked current profile

has two effects: the shear increases in the outer portion of the discharge, and the rational q surfaces shift toward larger minor radius, so that even the shear at the $q = 1$ surface becomes larger.

The change in current profile has a marked effect on the behaviour of the TAE mode. In the constant current discharge, the TAE activity, represented by the high pass filtered magnetic probe signal, rises immediately as the beam power reaches 10 MW. In the current ramp-down discharge, the onset of large TAE activity is delayed by about 200 ms after the end of the ramp-down. This delay is about the same as the time scale on which the current profile (ℓ_i) relaxes toward the constant current case.

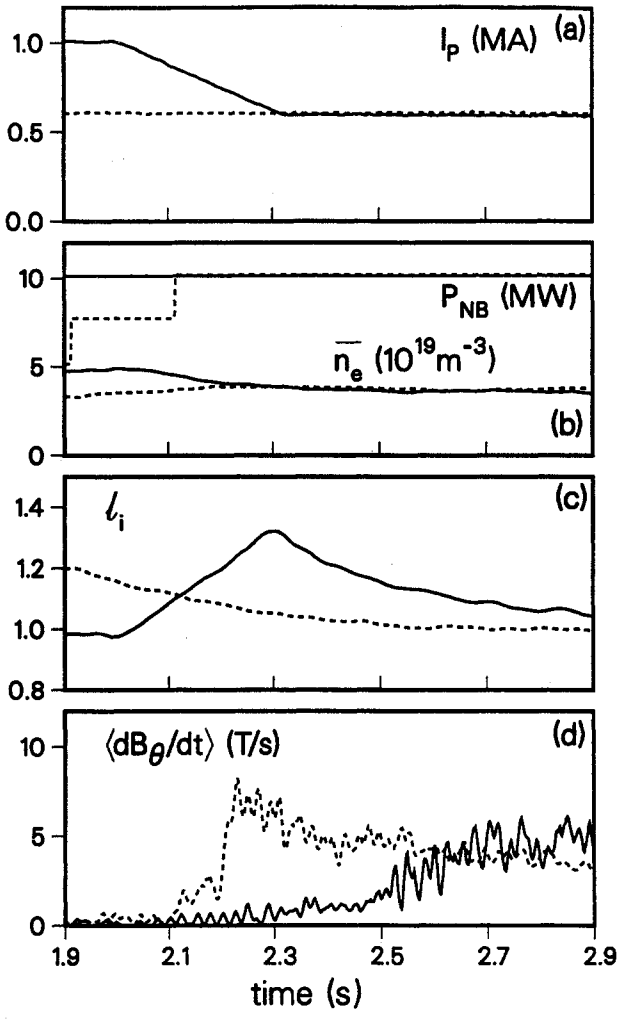

FIG. 15. Time traces for discharges with current rampdown (solid lines) and constant current (dashed lines). Traces: (a) plasma current I_p; (b) neutral beam power P_{NB} and electron density $\bar{n}_e$; (c) internal inductance ℓ_i from MHD equilibrium fits; (d) TAE activity (high pass filtered magnetic fluctuation amplitude $\langle dB_\theta/dt \rangle$, $90 < f < 250$ kHz). Discharges 71 531 and 71 517: $B_T = 1.0$ T.

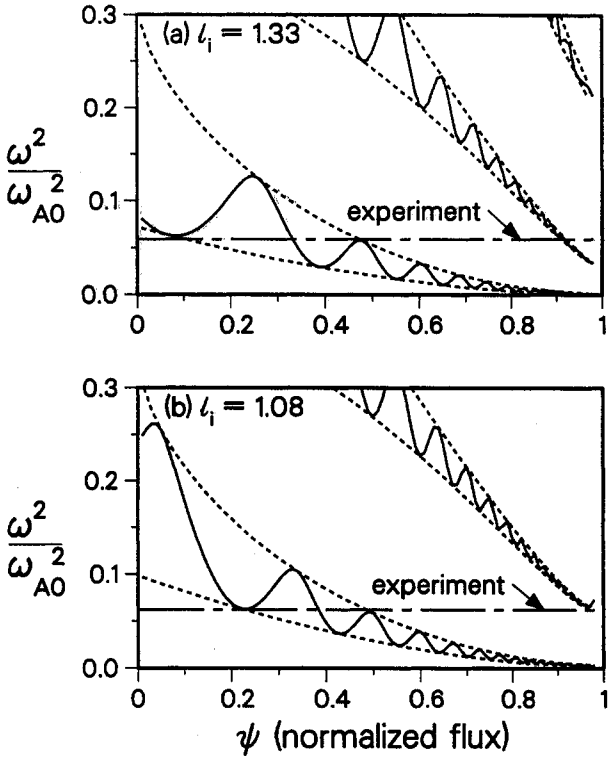

FIG. 16. Alfvén continuum spectra for high shear and low shear discharges. (a) High shear, immediately after current rampdown. (b) Low shear, constant current. Solid curves show the continuum spectrum for n = 3, and dotted curves show the envelope for the continua of all mode numbers, both calculated by CONT. The measured TAE frequency is also shown. Discharges 71 531 and 71 517.

The reduced TAE activity in the high shear (high ℓ_i) case is consistent with changes in the Alfvén continuum spectrum calculated by CONT. The spectra shown in Fig. 16 are calculated by using full equilibrium reconstructions with all available profile data. A flattened central fast ion pressure profile was assumed, similar to Case B in Fig. 5. In the high ℓ_i case immediately after the current ramp-down, the spectrum gap near the edge of the discharge is smaller, and the rational q surfaces have moved outward relative to the constant current case. Both of these changes increase the opportunity for damping by coupling to the continuum near the edge of the discharge. The experimentally observed TAE mode frequencies are also indicated. In the constant current case (Fig. 16(b)), the observed frequency misses the continuum at the edge of the plasma, providing no opportunity for continuum damping there; but in the current rampdown case (Fig. 16(a)), the observed frequency intersects the continuum, which should result in enhanced continuum damping.

Furthermore, coupling to the continuum near the edge of the discharge, which occurs only in the high ℓ_i case, may damp the mode more strongly than does continuum coupling near the centre, which occurs in both cases. In Eq. (6) for the continuum damping of a radially extended TAE mode, the functions $H_-(s)$ and $H_+(s)$ represent spatial integrals near the regions of continuum coupling at small and large minor radius respectively [10, 33]. Both are strongly decreasing functions of magnetic shear s. Thus, when continuum coupling occurs in the high shear region near the plasma edge, it is likely to make a larger contribution to the continuum damping rate than coupling in the central low shear region. Consistent with this prediction, other comparisons of experiment and theory [19] as well as the present current ramp experiment show that the existence and strength of observed TAE activity are better correlated with the presence or absence of a continuum crossing near the edge than with crossings near the centre. (In the simplified local analysis presented earlier in this paper, all contributions to the growth rate were evaluated by using experimental parameters at a single radial location. A more realistic result might be obtained by evaluating $H_-(s)$ and $H_+(s)$ at the continuum crossing locations calculated by CONT, but this is beyond the scope of the present work.)

The range of most unstable mode numbers is predicted to shift to higher n in the current rampdown case. The damping rates increase as expected when the analytic expressions of Section 4 are applied to the two equilibrium reconstructions. The continuum damping rate γ_c at $q = 3/2$ is approximately doubled in the current rampdown case, as shown in Fig. 17 for a representative toroidal mode number $n = 4$. There is very little change in the electron kinetic damping rate at a fixed value of q, because the increase in shear is offset by a decrease in electron temperature as the rational surfaces shift to larger minor radius. Consequently, the main effect of the increase in shear is to reduce the growth rate for low mode numbers, where continuum damping is important (see Fig. 18). Because of the proportionately greater change in damping at low n due to the enhanced continuum damping, the maximum total growth rate (evaluated at $q = 3/2$) shifts from $n = 2$–3 in the constant current case to $n = 3$–5 in the current ramp-down case.

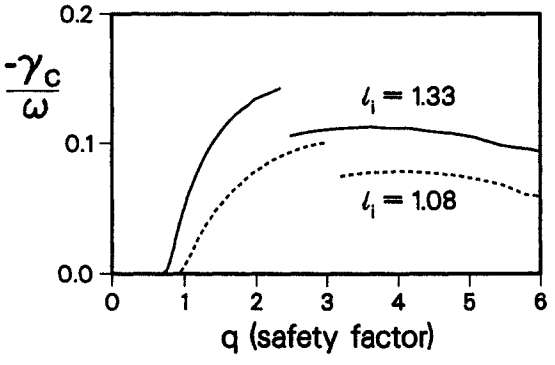

FIG. 17. Radial profiles of continuum damping rate γ_c for discharges with high shear (solid line) and low shear (dashed line). Here the damping rate is plotted versus q, *in order to compare the stability of modes at the same rational flux surface in cases with different spatial profiles of* q. *The break in each curve represents a transition between asymptotic high shear approximations and more exact numerical values in evaluating the terms in Eq. (5). Discharges 71 531 and 71 517.*

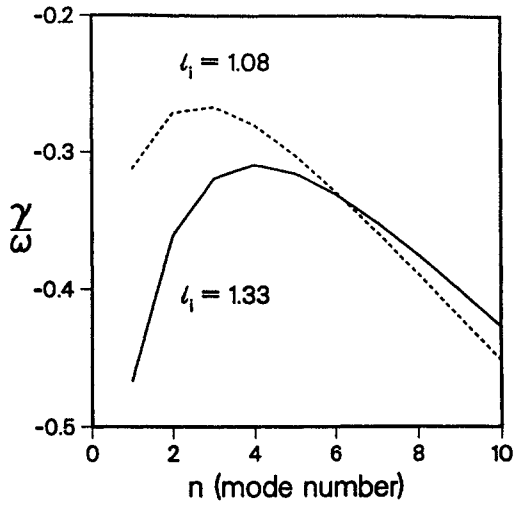

FIG. 18. Mode number dependence of the predicted growth rate in discharges with high shear (solid line) and low shear (dashed line). $\gamma = \gamma_f + \gamma_{damp}$ is evaluated at q = 3/2 *in discharges 71 531 and 71 517.*

Experimental evidence for this predicted shift in the TAE mode spectrum is seen most clearly in a set of discharges from another experimental run, with parameters very similar to the discharge 71 531 above. Here different timing of the fast digitizers in two identical discharges, 72 381 and 72 383, allows the evolution of the mode spectrum to be followed for 300 ms after the end of the current ramp-down. All other discharge parameters (beam power, plasma current, electron density, discharge shape) are constant during this time. As seen in Fig. 19, immediately after the rampdown the TAE spectrum consists primarily of mode numbers $n = 6$–8 at small amplitude. As the current profile relaxes toward lower shear and lower internal

inductance, the TAE spectrum evolves toward lower mode numbers and larger amplitudes. After 300 ms, the TAE spectrum consists primarily of mode numbers n = 3-5, at much larger amplitude. The inferred Doppler shift and Doppler corrected TAE frequency do not change much, indicating that the shift in the spectrum does not result from a change to a different mode location within the plasma. This change in the spectrum agrees well with the prediction of Fig. 18.

The good qualitative agreement of the predicted changes in the TAE spectrum with the experimental observations confirms the conclusions of Section 4, particularly the importance of continuum damping for low mode numbers. Previous experiments in DIII-D have shown that peaked current profiles are beneficial for MHD stability [48, 49] and energy confinement [50]; the same type of profiles also appear to be beneficial for stabilizing TAE modes. In the future, current profile control with RF current drive should allow such profiles to be sustained in steady state.

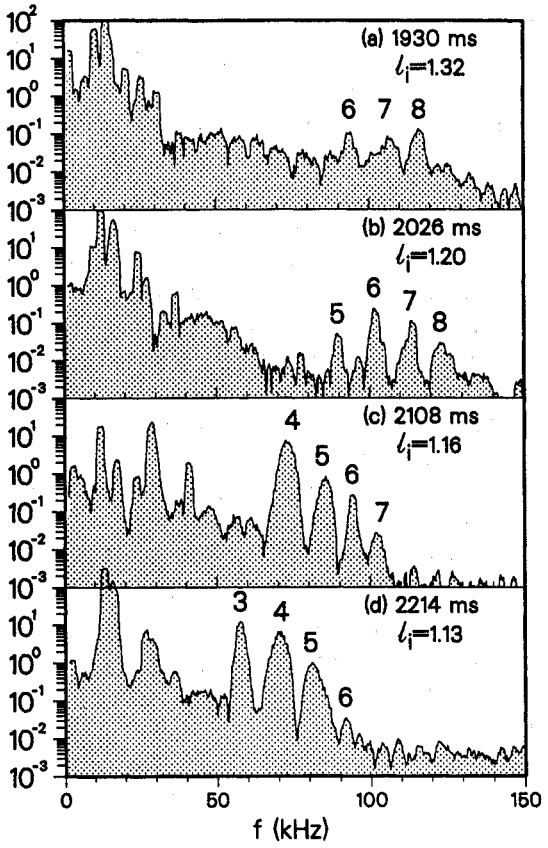

FIG. 19. Time evolution of the TAE mode spectrum during the current profile relaxation following a plasma current ramp-down. Toroidal mode numbers of TAE peaks are indicated. Discharges 72 381 and 72 383: B_T = 0.8 T, I_p = 0.6 MA, $\bar{n}_e = 4 \times 10^{13}$ cm^{-3}, P_{NB} = 10 MW.

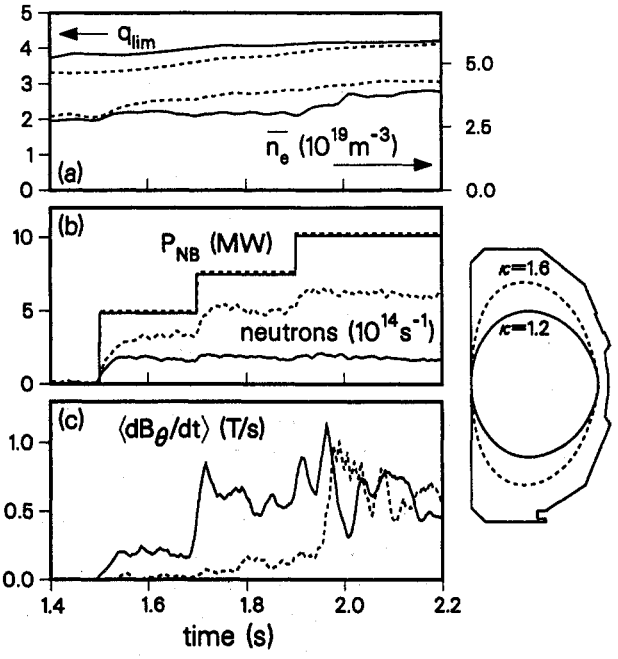

FIG. 20. Time traces for discharges with low elongation (solid lines) and high elongation (dashed lines). Traces: (a) limiter safety factor q_{lim} and electron density $\bar{n}_e$; (b) neutral beam power P_{NB} and neutron emission; (c) TAE activity (high pass filtered magnetic fluctuation amplitude, ⟨dB$_\theta$/dt⟩, 90 < f < 250 kHz). Discharges 72 393: κ = 1.2, I_p = 0.44 MA, and 72 389: κ = 1.6, I_p = 0.75 MA, both with B_T = 0.8 T.

5.2. Discharge shaping

Discharge elongation is found experimentally to have a stabilizing effect on TAE modes, which is qualitatively similar to the effect of increased magnetic shear described above. This may be the origin of the differences which have been noted between the observations in DIII-D and TFTR. Figure 20 shows time traces and discharge shapes for two discharges having similar parameters except the elongation. The reference case, discharge 72 389, has an elongation κ = 1.6, similar to the discharges discussed earlier. This is compared to discharge 72 393, which has an elongation κ = 1.2. The edge safety factor is kept the same in the two cases by reducing the plasma current for the low elongation discharge. The two cases have the same beam power and similar plasma density.

The TAE mode is destabilized at lower beam power in the low elongation case and may also cause greater fast ion loss. In the κ = 1.2 case, the TAE mode grows to large amplitude when the beam power reaches 7.5 MW, while in the κ = 1.6 the mode becomes large only at 10 MW of injected power. The neutron emission in the low elongation case is virtually

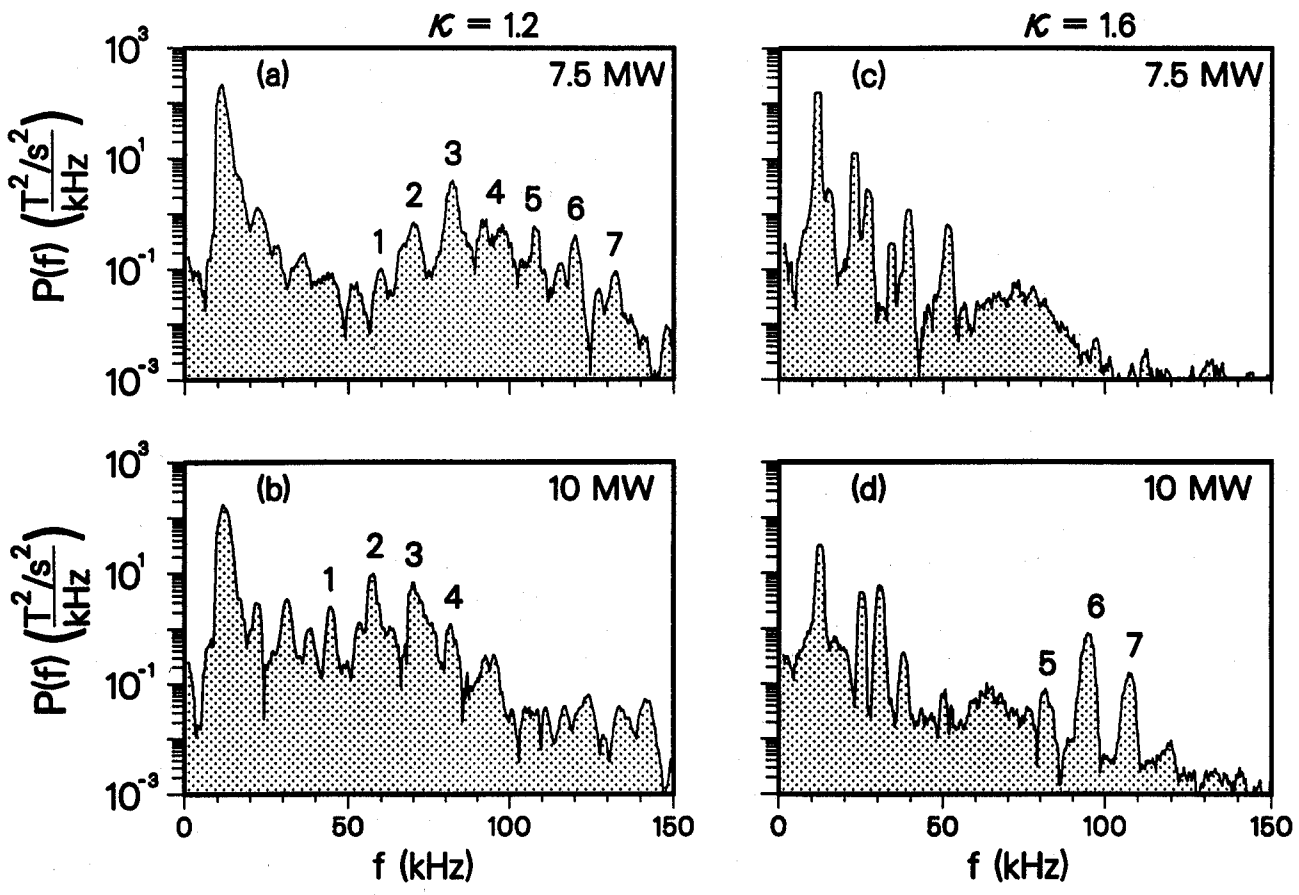

FIG. 21. Evolution of the TAE mode spectrum with increasing neutral beam power in discharges with (a, b) low elongation and (c, d) high elongation. Toroidal mode numbers of TAE peaks are indicated. Discharges 72 393 and 72 389.

constant as the beam power increases from 5 to 7.5 and 10 MW, indicating a large loss of fast ions, while in the high elongation case there is some indication of fast ion loss only as the power increases from 7.5 to 10 MW.

Corresponding differences are seen in the Fourier spectra of the magnetic probe signals, as shown in Fig. 21. At a beam power of 7.5 MW, the low elongation case has a set of TAE peaks dominated by mode numbers n = 2–5, while the high elongation case has no clear TAE spectrum. At 10 MW, the low elongation case has large TAE activity with mode numbers n = 1–3, while the high elongation case has smaller amplitude activity with n = 5–7. (Note that some of the TAE spectrum in the low elongation case falls below the 90 kHz cutoff of the high pass filtered magnetic probe signal, so the TAE amplitude for this case is actually larger than implied by Fig. 20.)

The same correlation between mode number and elongation is also seen in a broader database. In Fig. 22, the mode number with maximum amplitude at

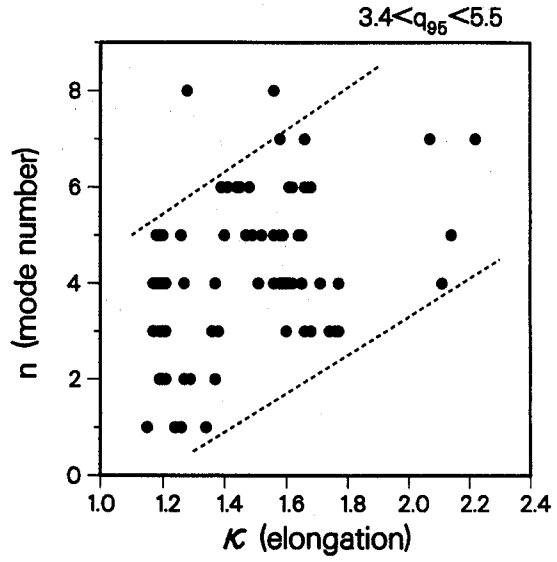

FIG. 22. Dominant TAE mode number versus discharge elongation for discharges with moderate q (3.4 < q_{95} < 5.5, where q_{95} is the safety factor at the 95% poloidal flux surface).

high frequency ($f \gtrsim 50$ kHz) has been plotted versus elongation for 89 discharges with moderate values of q. Although there is a wide range of observed mode numbers, there is also a clear upward trend with elongation. In particular, mode numbers $n = 1$ and $n = 2$ are dominant only in discharges with low elongation, $\kappa < 1.4$.

These observations are qualitatively consistent with the differences in details of the experimental results in DIII-D and TFTR. Many parameters (I_p, B_T, P_{NB}, $\bar{n}_e$, q, and κ) of the DIII-D low elongation case, discharge 72 393, are very similar to those of the TFTR discharges in which TAE modes have been reported [2, 13]. In the DIII-D low elongation case, the lower threshold in beam power is consistent with the somewhat lower threshold in fast ion beta in TFTR. The shift to lower toroidal mode numbers in the DIII-D low elongation case is also consistent with the mode numbers $n \sim 2$–3 observed in TFTR.

We can speculate on the reasons for this elongation dependence although the theories for driving and damping of TAE modes which were applied in Section 4 do not include non-circular discharge shapes. The shift to higher mode numbers which accompanies the improved stability at high elongation suggests stronger continuum damping of the low mode numbers, as in the current ramp-down case discussed above. The q profiles of the high and low elongation cases are quite similar to each other so that it is here difficult to attribute the increased damping to a change in the shear profile. We speculate that, when the TAE frequency does intersect the stable Alfvén continuum, the stronger shaping of the high elongation case improves the coupling to the continuum modes and thus increases the continuum damping. Numerical calculations indicate that triangularity can enhance the continuum damping of EAE modes by this mechanism [45], and similarly one would expect elongation and triangularity to enhance the continuum damping of TAE modes. However, verification of this speculation requires the development of a complete theory of continuum damping in non-circular geometry [44–46].

6. DISCUSSION

Although much work remains to be done, experiments and theory are converging toward an understanding of the stability of TAE modes. Several important physical mechanisms have been identified, and their relative importance has been estimated for experimental data. The qualitative behaviour of the experimental observations is consistent with theoretical expectations, and the quantitative agreement is reasonably good considering the limitations of the data and the theories. With the inclusion of realistic experimental geometry and finite beta effects in the theories, it should be possible in the future to make quantitative predictions of TAE mode stability for reactor relevant devices.

TAE modes driven by neutral beam ions were previously identified in DIII-D [1]. This identification has been further confirmed here by the dependence of the mode's stability on the beam injection angle and by the good agreement of the frequency with theoretical predictions as the Alfvén speed is varied by more than a factor of two.

The threshold in the ratio v_f/v_A implied by the resonance of the fast ions with the TAE mode has been confirmed in a single-parameter scan. However, the threshold is not a sharp one nor does it occur exactly at $v_f = v_A$. Possible explanations include pitch angle scattering of the fast ions [1], sideband coupling [8, 21, 22] by ions with $v_f/v_A \sim 1/3$, finite fast ion orbit width effects [34], and destabilization of a radially extended mode by fast ions located off the resonant flux surface [41]. More realistic calculations are planned of the fast ion distribution and its interaction with the predicted mode structure, in order to assess the importance of these effects for DIII-D experiments.

The main discrepancy noted in Ref. [1], the order of magnitude disagreement between the observed threshold in fast ion beta and predictions based on the electron Landau damping rate, has been resolved. The observed threshold in fast ion beta for destabilization of the TAE mode is within about a factor of two of estimates based on more recent theoretical predictions of the growth rate. The range of unstable mode numbers agrees well with predictions. Results of experiments to modify the TAE mode stability are also consistent with predictions.

Several damping mechanisms have been identified as important, depending on the mode number and the region of the plasma. The largest damping rate at all but the lowest mode numbers ($n \sim 1$–2) arises from non-ideal electron dynamics, including coupling to kinetic Alfvén waves. This is also the only theory out of those considered which has the appropriate mode number dependence to cut off the TAE mode at high mode numbers. Continuum damping becomes large at low mode numbers, leaving the observed intermediate range of mode numbers as the most unstable. Ion Landau damping may also become competitive in the

case of low mode numbers, particularly near the centre of the discharge where the ion temperature is high and the continuum damping is kept small by low magnetic shear.

The agreement within about a factor of two between estimates of the total predicted damping rate and fast ion driving rate can be considered good, in view of the many simplifying assumptions which were used in deriving the theories and adapting them to an easily calculated analytic form. In the future, removal of some of these assumptions from the theories will allow a more exact comparison with the experiment. Work is now in progress to calculate the low n continuum damping rate in a DIII-D equilibrium [46].

The greatest uncertainty in the experimental measurements is in the fast ion pressure profile. At present, the fast ion profile can only be estimated from classical deposition and slowing down calculations and the total neutron emission rate. Nevertheless, we have shown that the qualitative conclusions about the stability of the TAE mode are insensitive to the exact form assumed for the fast ion pressure profile. In the absence of a fast ion profile diagnostic, estimates of the experimental fast ion pressure could be improved by incorporating predictions of the fast ion loss in the presence of a TAE mode; these calculations are planned for DIII-D equilibria.

It should be possible to measure the total damping rate of the TAE mode directly, by exciting the mode with an antenna [5, 45] under conditions where the mode is stable. The width of the resonance observed as the antenna frequency is swept through the TAE frequency is proportional to the net damping rate. Such a measurement would allow the effects of current profiles or discharge shape to be studied, independent of uncertainties about fast ion profiles and velocity distributions or theories of fast ion drive.

Current profile control appears to be a promising approach to the stabilization of TAE modes through enhanced continuum damping. The transient current profile modification experiments described here have shown changes in the behaviour of TAE modes which are in qualitative agreement with damping theories. The centrally peaked current profile which is favourable for TAE mode stability has also been found to enhance energy confinement [50] and the high beta stability limit [48, 49]. In the future, the development of growth rate theories for realistic experimental geometries will allow the best current profiles for TAE stability to be determined, and profile control with RF current drive will allow such profiles to be sustained.

Discharge shaping (elongation and triangularity) should also have an important influence on the stability of TAE modes. Preliminary experiments in DIII-D suggest that increased alongation has a stabilizing effect, perhaps again by enhancing the continuum damping. These observations may also be consistent with TFTR experiments. The effect of discharge shape on TAE mode stability could be important for design of future devices such as ITER.

Although the threshold value of fast ion beta for destabilization is larger than initially expected, the TAE mode remains a potential problem for future devices such as ITER [51]. Fusion alpha particles in ITER are expected [52] to have a ratio $v_f/v_A \sim 1.3$–1.8 and a beta value $\beta_f \sim 0.4$–1.3%. At least part of this range lies in the regime where strong instability was observed in the DIII-D experiments. Similarly, the 1.3 MeV neutral beams proposed for noninductive current drive in ITER would have a ratio $v_f/v_A \sim 1.1$–1.6 which could be destabilizing, although the fast ion beta value $\beta_f \sim 0.1$–0.2% is below the 1% threshold observed in DIII-D. Therefore it is important to continue the development of stability theories in order to predict accurately the stability of TAE modes in ITER, as well as other devices. Similarly, it is important to continue the exploration of the stabilization of TAE modes by current profile control and other means.

7. CONCLUSIONS

Experiments show that the TAE mode exists in present day tokamaks and can cause significant loss of fusion products. The good agreement between measured and calculated frequencies gives credence to the theoretical description of this instability. A qualitative comparison of experimental data with various predictions for the growth rates shows that high mode numbers are stabilized by electron kinetic effects, while low mode numbers are stabilized by continuum damping and possibly by ion Landau damping. The dependence of continuum damping and electron kinetic damping on magnetic shear implies that current profile control can help to stabilize TAE modes, and preliminary experiments with a transiently peaked current profile support this conclusion. Experimental results indicate that discharge shaping may also have a stabilizing effect. In the future, improved means of current profile control (RF current drive, for example) should make it possible to avoid this instability, both in present experiments and in reactor relevant devices such as ITER.

ACKNOWLEDGEMENTS

The authors gratefully acknowledge the support by the DIII-D operations, neutral beam and physics groups. They would like to thank L.L. Lao, T.S. Taylor, H. Berk, R. Mett and J. Candy for helpful discussions. Assistance with data analysis was provided by E. Wilfrid, E. Carolipio and J. Manson.

This work was supported under USDOE No. DE-AC03-89ER51114.

REFERENCES

[1] HEIDBRINK, W.W., et al., Nucl. Fusion **31** (1991) 1635.
[2] WONG, K.L., et al., Phys. Rev. Lett. **66** (1991) 1874.
[3] CHENG, C.Z., et al., Ann. Phys. (N.Y.) **161** (1985) 21.
[4] FU, G.Y., CHENG, C.Z., Phys. Fluids B **2** (1990) 985.
[5] CHENG, C.Z., CHANCE, M.S., Phys. Fluids **29** (1986) 3695.
[6] FU, G.Y., VAN DAM, J.W., Phys. Fluids B **1** (1989) 1949.
[7] CHENG, C.Z., Phys. Fluids B **3** (1991) 2463.
[8] BETTI, R., FREIDBERG, J.P., Phys. Fluids B **4** (1992) 1465.
[9] ZONCA, F., CHEN, L., Phys. Rev. Lett. **68** (1992) 592.
[10] ROSENBLUTH, M.N., et al., Phys. Rev. Lett. **68** (1992) 596.
[11] BERK, H.L., et al., Phys. Fluids B **4** (1992) 1806.
[12] METT, R.R., MAHAJAN, S.M., Phys. Fluids B **4** (1992) 2885.
[13] WONG, K.L., et al., Phys. Fluids B **4** (1992) 2122.
[14] DUONG, H.H., HEIDBRINK, W.W., Nucl. Fusion **33** (1993) 211.
[15] DUONG, H.H., et al., Nucl. Fusion **33** (1993) 749.
[16] HEIDBRINK, W.W., et al., Phys. Fluids B **5** (1993) 2176.
[17] LUXON, J.L., DAVIS, L.G., Fusion Technol. **8** (1985) 441.
[18] TURNBULL, A.D., et al., in 1992 International Conference on Plasma Physics (Proc. Conf., Innsbruck, 1992), Vol. 16C, Part I, European Physical Society, Geneva (1992) 435.
[19] TURNBULL, A.D., et al., Phys. Fluids B **5** (1993) 2546.
[20] BIGLARI, H., CHEN, L., Phys. Rev. Lett. **67** (1991) 3681.
[21] BIGLARI, H., et al., Phys. Fluids B **4** (1992) 2385.
[22] BELIKOV, V.S., et al., Nuclear Fusion **32** (1992) 1399.
[23] HEIDBRINK, W.W., et al., Phys. Rev. Lett. **71** (1993) 855.
[24] LAO, L.L., et al., Nucl. Fusion **25** (1985) 1611.
[25] LAO, L.L., et al., Nucl. Fusion **30** (1990) 1035.
[26] CARLSTROM, T.N., et al., Rev. Sci. Instrum. **63** (1992) 4901.
[27] GOHIL, P.K., et al., Rev. Sci. Instrum. **61** (1990) 2949.
[28] WROBLEWSKI, D., LAO, L.L., Rev. Sci. Instrum. **63** (1992) 5140.
[29] PFEIFFER, W.W., et al., Nucl. Fusion **25** (1985) 655.
[30] CHU, M.S., et al., Phys. Fluids B **4** (1992) 3713.
[31] BERNARD, L.C., et al., Comput. Phys. Commun. **24** (1981) 377.
[32] TURNBULL, A.D., et al., Phys. Fluids B **4** (1992) 3451.
[33] ROSENBLUTH, M.N., et al., Phys. Fluids B **4** (1992) 2189.
[34] FU, G.Y., CHENG, C.Z., Phys. Fluids B **4** (1992) 3722.
[35] WILSON, J.R., et al., in Plasma Physics and Controlled Nuclear Fusion Research 1992 (Proc. 14th Int. Conf. Würzburg, 1992), Vol. 1, IAEA, Vienna (1993) 661.
[36] HEIDBRINK, W.W., SAGER, G., Nucl. Fusion **30** (1990) 1015.
[37] BERK, H.L., BREIZMAN, B.N., Phys. Fluids B **2** (1990) 2246.
[38] BERK, H.L., et al., Phys. Rev. Lett. **68** (1992) 3563.
[39] HSU, C.T., SIGMAR, D.J., Phys. Fluids B **4** (1992) 1492; SIGMAR, D.J., et al., Phys. Fluids B **4** (1992) 1506.
[40] BERK, H.L., Inst. for Fusion Studies, Univ. Texas, personal communication, 1992.
[41] BERK, H.L., et al., Phys. Lett. A **162** (1992) 475.
[42] FU, G.Y., VAN DAM, J.W., Phys. Fluids B **1** (1989) 2404.
[43] KERNER, W., et al., in Controlled Fusion and Plasma Physics (Proc. 18th Eur. Conf. Berlin, 1991), Vol. 15C, Part IV, European Physical Society, Geneva (1991) 89.
[44] POEDTS, S., et al., Plasma Phys. Control. Fusion **34** (1992) 1397.
[45] VILLARD, L., FU, G.Y., Nucl. Fusion **32** (1992) 1695.
[46] CHU, M.S., et al., in Plasma Physics and Controlled Nuclear Fusion Research (Proc. 14th Int. Conf. Würzburg, 1992), Vol. 2, IAEA, Vienna (1993) 71.
[47] GOROLENKO, N.N., SHARAPOV, S.E., Phys. Scr. **45** (1992) 163.
[48] STRAIT, E.J., et al., in Controlled Fusion and Plasma Physics (Proc. 18th Eur. Conf. Berlin, 1991), Vol. 15C, Part II, European Physical Society, Geneva (1991) 105.
[49] TAYLOR, T.S., et al., in Plasma Physics and Controlled Nuclear Fusion Research 1990 (Proc. 13th Int. Conf. Washington, 1990), Vol. 1, IAEA, Vienna (1991) 177.
[50] FERRON, J.R., et al., in 1992 International Conference on Plasma Physics (Proc. Conf. Innsbruck, 1992), Vol. 16C, Part I, European Physical Society, Geneva (1992) 55.
[51] TOMABECHI, K., et al., Nucl. Fusion **31** (1991) 1135.
[52] UCKAN, N.A., US ITER HOME TEAM, Fusion Technol. **21** (1992) 1444.

(Manuscript received 25 March 1993
Final manuscript received 31 August 1993)